Energy Consumption Minimization of Air-Water Visible Light Communications

Wenzhi Du

Department of Electronic and Electrical Engineering

University of Sheffield

A thesis submitted in partial fulfilment of the requirements for the degree of

Doctor of Philosophy

August 12, 2024

Abstract

As offshore industries and the internet of underwater things continue to expand, air-to-water communication is needed to connect various underwater sensors and things to the outside world. Long term energy-efficient air-to-water wireless communications have been increasingly attracting attention due to the need of military application, marine life studying, and climate monitoring. However, it is always a challenge to communicate directly across the air-water interface by a single type of wireless signal. Acoustic waves used underwater have a very low bandwidth and result in a high delay especially in the air, while electromagnetic waves have a high attenuation while travelling underwater and result in a short communication distance and a higher energy consumption. Traditionally, the communication between air and underwater requires an interface such as a floating base-station to serve as a relay. However, this solution can be costly, lack of responsiveness and even unacceptable in some situation. To overcome the air-water interface, visible light communication (VLC) has been considered for direct air-water communications. Compared with acoustic and radio frequency (RF) communications, VLC has higher bandwidth and lower energy consumption. As a result, VLC can achieve a higher data rate for air-water communication than acoustic or RF communications.

In this thesis, low-power air-water communications are investigated, while considering that the underwater nodes may be drifted by water currents within a certain range from their default positions. Therefore, diffused-line-of-sight VLC using light emitting

diode (LED) is considered since it generally has a wider beam angle and results in an acceptable coverage area, and it has a lower transmission power consumption compared to lasers. This thesis studies two air-water VLC systems as follows. In the air-to-water VLC system, an LED transmitter carried by a unmanned aerial vehicle (UAV) hovering above the water transmits data of a certain volume to an underwater receiver in a deep water scenario. In the water-to-air VLC system, an UAV carrying a photodiode receiver hovers above the water and receives a certain amount of VLC signals from an underwater LED transmitter in a shallow water scenario.

To solve the light propagation path in order to obtain the light propagation distances and the coverage area, the air-water interface are mathematical modelled for both air-water VLC systems. In the air-to-water VLC system, Stokes's third-order theory are used to model the water surface elevation for the deep water scenario, while in the water-to-air VLC system which consider the shallow water scenario, the Boussinesq equations and Korteweg-de Vries equation are adopted. The signal-to-noise ratio (SNR) at the receiver and the channel capacity are derived while considering the transmittance that represents how much light can penetrate the water surface, the receiving area of the receiver and the underwater noise terms.

To fulfil the requirement of long-term sustainable air-water VLC, in both air-water VLC systems, the energy consumption minimization problems are formulated and solved by the proposed algorithms. More specifically, in the air-water VLC system, a sequential quadratic programming based algorithm is devised to minimize the total energy consumption of the UAV by optimising the LED transmit power while guaranteeing that the average received SNR at the underwater receiver is above the required SNR for all possible receiver positions within the light coverage, while in the water-to-air VLC system, an algorithm is proposed to minimize the total energy consumption of the VLC system by jointly optimising the LED transmit power and the UAV height

while guaranteeing that the average received SNR at the receiver is above the required SNR for all possible underwater transmitter positions that meet the light coverage requirement for the receiver.

For both work in air-water VLC, the proposed algorithm outperforms the other benchmark strategies of choosing the LED transmit power or the UAV height in minimizing the energy consumption while keeping the transmission time at the same level. Specifically, in the air-to-water VLC system, for the underwater receiver depth of 10 meters, the optimized LED transmit power can reduce the total energy consumption of the UAV by up to 47% as compared to that of LED transmitting at the maximum power, and in the water-to-air VLC system, for the underwater transmitter depth of 10 meters, the optimal values of the LED transmit power and the UAV height can save up to 32% of the total energy consumption of the system as compared with transmitting at a random power level and placing the UAV at a random height.

Acknowledgment

I would like to express my endless gratitude to those who helped me while pursuing my study at this prestigious university. Without their sincere help, it would be impossible for me to complete my study.

First and foremost I am extremely grateful to my first supervisor Prof. Xiaoli Chu, for her invaluable advice, continuous guidance, and patience during my PhD study. Her immense knowledge and plentiful experience have provided me with constant encouragement throughout my academic research and daily life. Furthermore, I would like to thank my second supervisor Prof. Jie Zhang for his help and suggestions on my study.

I would like to extend my sincere thanks to my colleagues Dr. Yang Liu and Dr. Na Tang, for their kind help and technical support on my study.

Finally, I would like to express my gratitude to my parents for their unwavering support and encouragement.

Table of Contents

List of Figures

List of Tables

List of Abbreviations

APD avalanche photodiode 30

ASK amplitude shift keying 24

AUV autonomous underwater vehicle 32

AWGN additive white Gaussian noise 15

BCH Bose–Chaudhuri–Hocquenghem 66

BER bit error rate 7

DLOS diffused-line-of-sight 2

EM electro-magnetic 2

FEC forward error correction 66

IM/DD intensity modulation/direct detection 6

IoUT internet of underwater things 1

Chapter 1

Introduction

1.1 Research Background and Motivation

Owing to growing underwater activities, e.g., undersea oil & gas exploration, and the internet of underwater things (IoUT) [1], which are expected to connect the outside world to various underwater nodes, sensors and autonomous underwater vehicles, energy-efficient air-to-water wireless communications are urgently needed by the industry, military, and scientific communities. Traditionally, the communication between air and underwater requires a relay such as a floating base-station that receives radio frequency (RF) signals from a transmitter above water and transmits acoustic [2] or optical signals [3,4] to an underwater receiver, but this solution can be costly since it requires a boat or a buoy that is equipped with both radio and acoustic/optical modems. Also, there are some intrinsic technical limitations by using a buoy as a relay. Firstly, the transmission rate of the relay-based air-water system is limited by the acoustic bandwidth which is in the order of tens of kbps [5]. Secondly, there is an unacceptable delay of communication that measured in seconds due to the low propagation speed of acoustic wave which is about 1.5×10^3 m/s [6]. Thirdly, the buoy relays are susceptible

to the effects of water movements and potential collisions with maritime vessels [7]. Moreover, it can be a lack of responsiveness and even unacceptable in some situations. For example, a wide-range search and rescue mission in ocean normally requires quick response and placing relay base-station is not feasible. For military applications, a floating base-station will be easily discovered and thus expose underwater nodes such as submarines [8]. For the above reasons, recent research is mainly focused on air-water communication without an interface to better serve related applications.

To overcome the air-water interface, different approches have been stuied including magnetic induction (MI) [9–12], electro-magnetic (EM) [13,14], translational acoustic-RF communication (TARF) [15] and laser-induced acoustic (LIA) [16, 17]. The main benefit of MI and EM communication methods lies in their ability to tolerate the turbulence, bubbles and turbidity in the water, but the communication systems require large antennas with high transmit power due to severe path loss of RF signals [9]. TARF is in early stage and only support water-to-air communication [15]. LIA requires a low energy consumption for laser pulse and is easier to set up the underwater communication compared to a laser link by converting the optical signal to acoustic signal, but LIA is still in early stage and only experiments in small transmission distance (less than 1 meter) have been done [16].

Visible light communication (VLC) has also been considered for air-water communications. Compared with acoustic and RF communications, VLC has higher bandwidth and lower energy consumption [18]. As a result, VLC can achieve a higher data rate for air-water communication than acoustic or RF communications [19]. According to Table 1 in [19], diffused-line-of-sight (DLOS) optical air-to-water links can achieve data rates of around 30Mbps, while relay-based air-to-water communication that uses an RF link in the air and an acoustic link in the water has a data rate of a few kbps. Although the communication range of VLC is typically limited to below 50 meters underwater [20],

it can provide a sufficiently large coverage via diffuse light transmission, e.g., by using light emitting diodes (LEDs).

In the realm of VLC, there are typically two distinct technologies: line-of-sight (LOS) and DLOS. Laser diode (LD) and LED are the common light sources employed for establishing LOS and DLOS air-water VLC links, respectively. In LOS VLC, the light source emits a narrow beam with a low divergence angle between the transceivers, resulting in a highly directional and intense beam that facilitates long-range communication. The primary challenge with LOS is the need to maintain precise alignment between the transmitter and the recevier [19]. On the other hand, in DLOS VLC, the light source such as LED transmitter generally has a wider beam angle and results in a larger coverage area, in the trade-off of a lower transmission rate.

To study the air-water by using VLC, many works have been done by the researchers. The mathematical models of the air-water interface [21, 22] enable the analysis of the light propagation path and light power loss due to refraction and reflection. The attenuation of water [23–26], turbulence [27–29] and bubbles [30] in the water, as well as the underwater noises [24, 25, 31] are studied in order to understand the channel in a air-water VLC link. The modulation schemes are experimental studied and compared in [32]. A concatenated Reed Solomon-Low Density Parity Check coding is proposed in [33] to improve the reliability of a water-to-air VLC link. A beam tracking system is proposed to mitigate the impact of water wave [34]. An optical camera system is presented in [35] to reduce the impact of bubble in the water. The security of the VLC link is analysed and enhanced in [36, 37].

To deal with the energy-related challenge of VLC system, green computing and green energy are studied in [38–40], and simultaneous lightwave information and power transfer (SLIPT) is proposed as a potential technology to recharge batteries for IoUT devices during the VLC transmission.

The motivation of this research is to fulfil the requirement of long-term sustainable air-water VLC link for marine life monitoring and studying applications, and focus on minimizing the energy consumption of the air-water VLC system. Specially, this research project focuses on low-power air-water communications while considering that the underwater nodes may be drifted by water currents within a certain range from their default positions. Therefore, DLOS VLC using LEDs is considered to achieve an acceptable coverage area.

1.2 Research Challenges and Objectives

Air-to-water VLC is still facing some critical challenges that need to be tackled. Firstly, the water surface is often wavy and the shape of the surface wave is time-varying depending on water depth and wind speed. The wavy water surface affects the proportion of light that passes through the air-water interface due to reflection and the underwater propagation path due to refraction, thus affecting the transmission distance and coverage area underwater. Secondly, there are various underwater noise sources, such as solar interference and thermal noise, which may degrade the signal-to-noise ratio (SNR) and channel capacity. Thirdly, the required LED transmission power increases with the depth of the underwater receiver and the attenuation coefficient of water for achieving a certain communication performance, while the unmanned aerial vehicle (UAV) that carries the LED transmitter is typically energy limited.

In this thesis, the considered air-water VLC application is described as follows: an underwater node equipped with a VLC transceiver is deployed at a given depth in the water to collect data on marin life, water condition, etc., by its sensor for a long-time period. The data type of the application can be text, audio or image depending on the underwater node sensor and its task. An UAV is dispatched periodically to collect

the data from the underwater node or send task commands to the underwater node by its carried VLC transceiver. The VLC transceiver includes an LED transmitter and a photodiode receiver. The UAV knows the default position of the underwater node and hovers directly above it for transmitting/receiving a certain amount of data by VLC. The hovering time, and consequently the energy consumption of the UAV, increases with the amount of data that needs to be transmited. Although only one underwater node is considered in the system model in this thesis, the UAV may need to fly to other locations to transmit/collect data to/from other underwater nodes before it can fly back to its base to be recharged. Therefore, the UAV energy consumption minimization problem is considered in this application.

In this project, an air-to-water VLC system and a water-to-air VLC system are analysed respectively. In the air-to-water VLC system, the first objective is to mathematically model the air-water interface by considering a deep water wave and analytically derive the light propagation path. The second objective is to formulate and solve an energy consumption minimization problem which considers both the energy used for VLC by the LED transmitter and the UAV propulsion energy consumption when hovering above the water at a given position by optimizing the LED transmit power, while guaranteeing that the average received SNR is above the required SNR.

In the water-to-air VLC system, the shallow water wave is considered, and the first objective is to mathematically model this type of air-water interface and analytically solve the light propagation path. The second objective is formulate and solve an energy consumption minimization problem considering both the energy used by the underwater LED transmitter and the UAV propulsion energy consumption by jointly optimizing the LED transmit power and the UAV height, while guaranteeing that the average received SNR is above the required SNR.

1.3 Thesis Contributions and Publications

This thesis studies the low-power air-to-water and water-to-air VLC while considering that the underwater note may be drifted by water currents within a certain range from its default position. Hence, LEDs are chosen as they can emit light in more diffused beams (resulting in larger coverage areas) with lower transmission power than lasers. More specifically, in the air-to-water VLC system, an LED transmitter carried by an UAV hovering above the water needs to transmit data of a certain volume to an underwater receiver in a deep water scenario. Based on the intensity modulation/direct detection (IM/DD) scheme that is widely used in optical communications, the on-off keying (OOK) non-return-to-zero (NRZ) modulation is adopted for the VLC link. A sequential quadratic programming (SQP)-based algorithm is devised to minimize the total energy consumption of the UAV by optimising the LED transmit power while guaranteeing that the average received SNR at the underwater receiver is above the required SNR for all possible receiver positions within the light coverage. In the water-to-air VLC system, an UAV carrying a photodiode receiver hovers above the water and receives a certain amount of VLC signals from an underwater LED transmitter in a shallow water scenario, and an algorithm is proposed to minimize the total energy consumption of the VLC system by jointly optimising the LED transmit power and the UAV height while guaranteeing that the average received SNR at the receiver is above the required SNR for all possible underwater transmitter positions that meet the light coverage requirement for the receiver.

In air-to-water VLC, the potentially wavy water surface is modelled by using Stokes's third-order theory [21] and the light incident point on the water surface is analytically derived for a given UAV position and all possible positions of the underwater receiver that fall inside the light coverage. In water-to-air VLC, the air-water

interface is modelled by using Boussinesq equations and Korteweg-de Vries (KdV) [22] equation and the light incident point on the water surface is analytically derived for a given UAV position and all possible positions of the underwater transmitter that meet the light coverage requirement for the receiver. Based on these models while considering that the underwater notes may be drifted by water currents within a certain range from its default position, the transmission distances above and under water and the angle between the light propagation direction and the optical axis of the receivers are obtained.

By mathematically model the water surface and solving the light propagation path, the SNR at the receiver and the channel capacity for OOK-NRZ are derived while considering the transmittance that represents how much light can penetrate the water surface, the receiving area of the receiver and the underwater noise terms. Based on the derived expressions of the received SNR and the channel capacity, the time required for the LED transmitter to transmit a given amount of data to the receiver and the total energy consumption that includes both the energy used for VLC by the LED transmitter and the UAV propulsion energy consumption when hovering above the water at a given position can be calculated.

Leveraging the above analytical results, for the air-to-water VLC the UAV energy consumption minimization problem is formulated for transmitting a certain volume of data to the underwater receiver at a given depth by optimizing the LED transmit power while ensuring the received SNR is sufficient for a target bit error rate (BER). The UAV energy consumption minimization problem is solved by exploiting the trade-off between saving LED transmission power and saving UAV propulsion energy, e.g., reducing the LED transmit power increases the required data transmission time and leads to a higher UAV propulsion energy consumption. Since the incident point of the light propagation path on the water surface cannot be determined analytically, a

SQP-based algorithm is devised to numerically solve the optimization problem. For the water-to-air VLC, the total energy consumption minimization problem is formulated for the underwater LED transmitter at a given depth transmitting a certain volume of data to the receiver at the UAV while ensuring the received SNR is sufficient for a target BER. The total energy consumption minimization problem is solved by the proposed algorithm that jointly optimizing the LED transmit power and the UAV height.

Simulation results show that for the air-to-water VLC system the optimized LED transmit power obtained by the proposed algorithm can reduce the UAV energy consumption by around 47% for the underwater receiver depth of 10 meters as compared to the benchmark schemes, without increasing the transmission time for transmitting a certain data volume, and for the water-to-air VLC system the proposed algorithm can save around 32% of the total energy consumption of the system as compared with transmitting at a random power level and placing the UAV at a random height.

As at this thesis is written, the papers that have been submitted and under preparation for submission are list below.

1. W. Du, Y, Liu and X. Chu, "Energy Consumption Minimization of Air-to-Water Visible Light Communications," (Submitted to IEEE Internet of Things Journal).

2. W. Du, Y, Liu and X. Chu, "Energy Consumption Minimization of Water-to-air Visible Light Communications," (Under preparation for submission).

1.4 Thesis Organisation

The rest of the thesis is organized as follows.

In Chapter 2, the fundamental concepts related to the research and literature review of the related works is written. To provide a better understanding of our research topics,

it is essential to describe the associated foundational concepts before delving into the literature reviews. The topics discussed in the fundamental concepts include the water surface model, VLC signal propagation, reflection and refraction of light, transmittance cause by the water surface reflection, attenuation coefficient of water, turbulence and bubbles in the water, noises at the receiver and the common VLC modulation schemes. For the literature review, the related works on air-to-water communication and water-to-air communication are discussed, and extended to recent UAV-assisted air-water communication and energy-related air-water communication works.

In Chapter 3, an air-to-water DLOS VLC system, as the first research model is presented, where the LED transmitter carried by an UAV above the water transmits optical signal to an underwater receiver. The deep water air-water interface is mathematically modelled and the light propagation path is solved. A SQP-based algorithm is devised to solve the formulated UAV energy consumption minimization problem by optimizing the LED transmit power.

In Chapter 4, a water-to-air DLOS VLC system, as the second research model is presented, where an underwater LED transmitter sends optical signal to a receiver carried by the UAV in the air. The shallow water air-water interface is mathematically modelled and the light propagation path is solved. The proposed algorithm solve the formulated energy consumption minimization problem of the system by optimizing the LED transmit power and the UAV height.

Finally, the conclusions of the work done in Chapter 3 and 4 and the recommendation for future work is highlighted in Chapter 5.

Chapter 2

Fundamental Concepts and Literature Review

2.1 Fundamental Concepts

2.1.1 Water Surface Model

In most realistic scenarios, the water surface is not flat and there is a wave at the air-water interface due to the effects of wind. The characteristics of surface waves are primarily influenced by factors such as water depth and wind speed. It is challenging to find an exact elevation equation to describe these water waves. For simplicity, the surface elevation is typically considered to be a cnoidal function.

The water wave type is defined by the relationship between the water depth and the wavelength of the water wave. Let d denote the water depth and λ_w denote the wavelength of the water wave. For shallow water waves where the wavelength is greater than the water depth [41], i.e. $\lambda_w > d$, the Boussinesq equations and KdV equation have been employed as the popular mathematical model to describe and analyze the the behavior of water surface wave, which is expressed as [22]

$$f(x,t) = f_A + H\mathrm{dn}^2\left(\frac{x - c_w t}{f_B}|m\right), \tag{2.1}$$

$$f_A = \frac{H}{m}\left[1 - m - \frac{E(m)}{K(m)}\right], \tag{2.1a}$$

$$f_B = \frac{\lambda_w}{2K(m)} = d\sqrt{\frac{4md}{3H}}, \tag{2.1b}$$

$$c_w = \sqrt{gd}\left\{1 + \frac{H}{md}\left[1 - \frac{m}{2} - \frac{3E(m)}{2K(m)}\right]\right\}, \tag{2.1c}$$

where x is the horizontal coordinate of a point on the water surface, t is time, H is wave height, dn is the Jacobi DN elliptic function, c_w is the phase speed of water wave, $m \in [0, 1]$ is the square of elliptic modulus, $E(m)$ is the complete elliptic integral of the second kind, $K(m)$ is the complete elliptic integral of the first kind, λ_w is the wavelength of water wave, d is water depth and g is the gravitational acceleration.

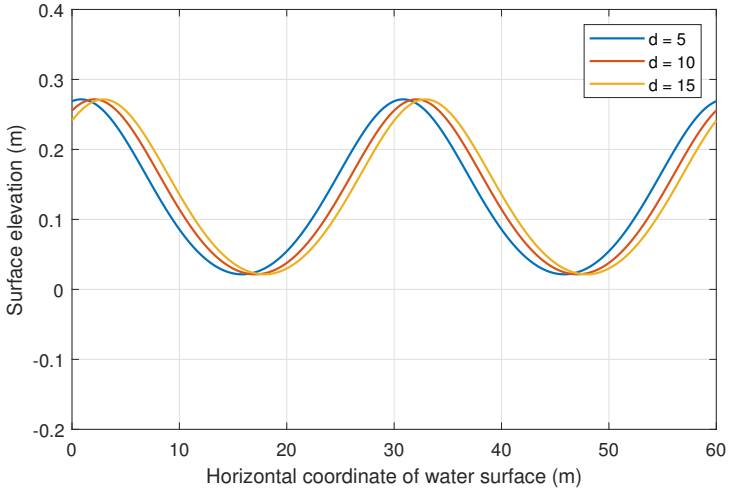

Figure 2.1: The surface elevation versus the horizontal coordination of the water surface for shallow water wave at different water depth for $m = 0.5$, $H = 0.5$m, $\lambda_w = 30$m and $t = 0.3$s.

From (2.1c), the water depth has an effect on the phase speed of water wave. In this water surface model, the water wave moves horizontally from left to right. From

Fig. 2.1, the phase speed of water wave increases as the water depth becomes larger.

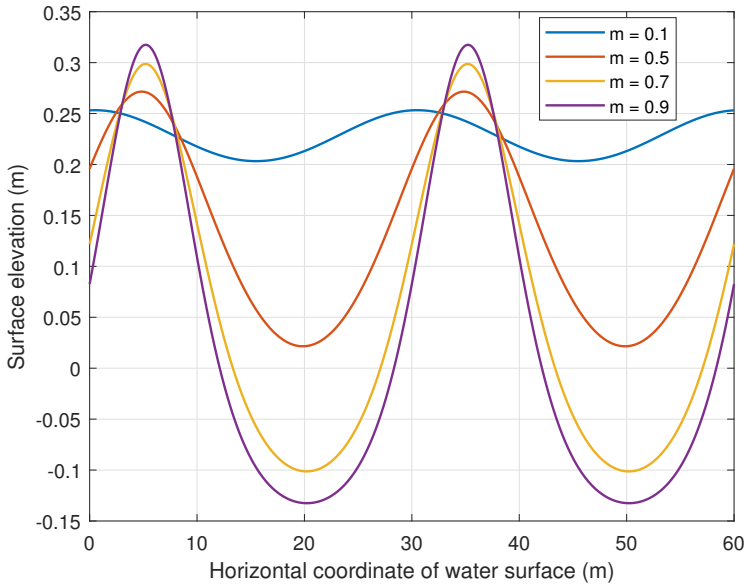

Figure 2.2: The surface elevation versus the horizontal coordination of the water surface for shallow water wave at different square of elliptic modulus for $d = 15$m, $H = 0.5$m, $\lambda_w = 30$m and $t = 0.5$s..

The square of elliptic modulus m describes the shape of the water wave. As shown in Fig. 2.2, when m approaches 1, the peaks of the water wave become sharper, and the troughs become flatter. For lower values of m, the water wave presents a more sinusoidal pattern.

On the other hand, if the water depth is larger than the wavelength of the water, i.e. $d > \lambda_w$, it is considered to be a deep water wave [41]. For deep water waves, Stokes's wave theory is commonly applied for the water surface [21].

$$
\begin{aligned}
f(x,t) =& \alpha \left\{ \left[1 - \frac{1}{16}(k\alpha)^2 \right] \cos(kx - \omega t) \right. \\
&+ \frac{1}{2}(k\alpha) \cos\left[2(kx - \omega t)\right] \\
&\left. + \frac{3}{8}(k\alpha)^2 \cos\left[3(kx - \omega t)\right] \right\} + O\left[(k\alpha)^4\right], \qquad (2.2)
\end{aligned}
$$

$$
k = \frac{2\pi}{\lambda_w}, \qquad (2.2a)
$$

$$
\omega = k \left[1 + \frac{1}{2}(k\alpha)^2 \right] \sqrt{\frac{g}{k} + O\left((k\alpha)^4\right)}, \qquad (2.2b)
$$

where x is the horizontal coordinate of a point on the water surface, t is time, k is the angular wavenumber, α is the first-order wave amplitude, $k\alpha \in [0, 1]$ is the wave steepness, ω is the angular frequency of the water wave, $O((k\alpha)^4)$ is the sum of least significant terms, λ_w denotes the wavelength of water waves, and g is the gravitational acceleration.

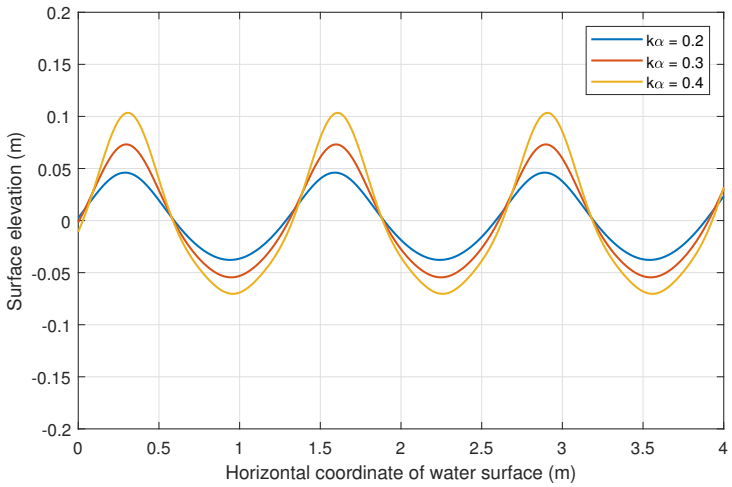

Figure 2.3: The surface elevation versus the horizontal coordination of the water surface for deep water wave at different wave steepness for $\lambda_w = 1.3$m and $t = 0.2$s.

Fig. 2.3 shows the horizontal coordination of the water surface versus the surface

elevation for deep water wave at different wave steepness $k\alpha$. The typical value of $k\alpha$ is below 0.5 [42]. From Fig. 2.3, when $k\alpha$ becomes larger, the peaks of the water wave become steeper, and the amplitude becomes larger.

Another commonly used time-varying water surface equation uses Gerstner waves [43, 44] to express a composite wave consisting of N sine waves. Gerstner waves were initially discovered as an approximate solution to the fluid dynamic equations. The physical model aims to characterize the surface by describing the motion of individual points on the surface.

For a point on the flat water surface that is not displaced by any wave, its position in the horizontal plane is $\boldsymbol{x} = (x_0, z_0)$ and it height is $y_0 = 0$. As a composite wave consisting of N sine waves passes by, the point on the surface displaced at time t is given by [44]

$$\boldsymbol{x} = x_0 - \sum_{i=1}^{N} (\boldsymbol{k}_i \lambda_i / 2\pi) A_i \sin(\boldsymbol{k}_i x_0 - \omega_i t + \phi_i), \tag{2.3}$$

$$y = \sum_{i=1}^{N} A_i \cos(\boldsymbol{k}_i x_0 - \omega_i t + \phi_i), \tag{2.4}$$

where $\boldsymbol{k}_i$ is the wavevector that points in the direction of travel of the wave. λ_i is the length, A_i is the amplitude, ω_i is the frequency, and ϕ_i is the phase of the ith wave.

Gerstner waves provide an exact description of the deep water wave, but the realizability is the problem, while the Stokes's wave theory is tractable [45]. For shallow water waves, the Boussinesq equations and KdV equation are more accurate since it considers the effect of the water depth [22]. Therefore, in this thesis, the Stokes's wave theory is used for deep water waves and the Boussinesq equations and KdV equation are used for shallow water waves.

2.1.2 VLC Signal Propagation

Like in most of the optical wireless communication (OWC) systems, IM/DD is commonly used in VLC systems [46], since it has a low cost and implemented complexity.

The transmitted information bits are recovered by the receiver using a matched filter for direct-detection [47]. The resulting electrical signal sampled at the output of the matched filter can be expressed as [48]:

$$Y_i = \eta I X_i + n_i, \tag{2.5}$$

where η is the optical-to-electrical conversion coefficient, I is the light intensity of the received signal, $X_i \in \{0, 1\}$ is the ith information bit, and n_i is the additive white Gaussian noise (AWGN) in the ith bit period. The AWGN has a zero mean and variance σ_n^2. According to [48], η is given by:

$$\eta = \frac{\gamma T_b q \lambda}{hc}, \tag{2.6}$$

where γ is the quantum efficiency of the photodetector at the receiver, T_b is the bit interval, $q = 1.6 \times 10^{-19}$coulombs is the elementary charge, λ is the wavelength of the light signal, $h = 6.6261 \times 10^{-34}$J is Plank's constant, and $c = 2.25257 \times 10^{8}$m/s is the speed of light.

2.1.3 Transmittance

When the light passes through the interface of different mediums, there is a percentage of light power loss due to the reflection by the interface. Let τ denote the transmittance which represents how much light can penetrate the interface, and r be the reflectance which represents how much light is reflected due to the interface. The relationship

between them is given by [49]:

$$\tau = 1 - r. \tag{2.7}$$

If a light travels from a medium with refractive index of n_1 to a medium with refractive index of n_2, for an unpolarized light source, the reflectance can be expressed based on Fresnel equation [49] as follows:

$$r = \frac{r_s + r_p}{2}, \tag{2.8}$$

$$r_s = \left| \frac{n_1 cos\theta - n_2 cos\varphi}{n_1 cos\theta + n_2 cos\varphi} \right|^2, \tag{2.9}$$

$$r_p = \left| \frac{n_1 cos\varphi - n_2 cos\theta}{n_1 cos\varphi + n_2 cos\theta} \right|^2, \tag{2.10}$$

where r_s and r_p are the reflectance coefficients of s-polarized light and p-polarized light, respectively; θ and φ are the angle of incidence and the angle of refraction, respectively;

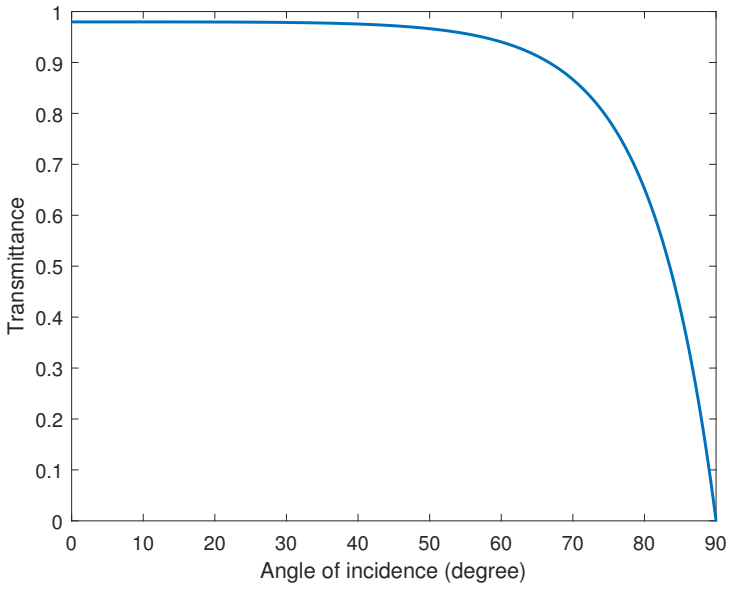

Figure 2.4: Angle of incidence versus the transmittance for air-to-water light propagation.

Fig. 2.4 shows the angle of incidence versus the transmittance for the scenario that the light travels from the air to the water across the air-water interface by using (2.7)–(2.10). As shown in Fig. 2.4, the transmittance is close to 1 for any angle of incidence below 60 degrees and then drops rapidly when the angle of incidence increases beyond 60 degrees. In our VLC system model using LED, increasing the beam angle of the LED results in a larger light coverage area, but also leads to a greater angle of incidence at the edge of the LED beam. For a flat water surface, the largest angle of incidence is half of the LED beam angle. However, for a wavy water surface, the angle of incidence is time varying with the change of the water wave. In this thesis, the LED beam angle is considered to be 45 degrees because the simulation results show that, with this LED beam angle value, 99.6% of the incident angles are smaller than 60 degrees. In this case, the transmittance is close to 1 and the received light power is minimally attenuated due to the reflection by the interface, while maintaining a sufficiently large light coverage area.

2.1.4 Attenuation coefficient of Water

The propagation loss factor, L_p as a function of wavelength and distance, under the Beer-Lambert law is given by

$$L_p(\lambda, z) = \exp^{-c(\lambda)z}, \tag{2.11}$$

where $c(\lambda)$ denotes the attenuation coefficient of water, λ is the wavelength of the light source, and z is the light propagation distance underwater.

As shown in Fig. 2.5 from [24], the attenuation coefficient of water $c(\lambda)$ are classified according the Jerlov water types. O1 to O3 represent the clear ocean values, where the lower number designates the more clear water type, and C1 to C10 similarly represent

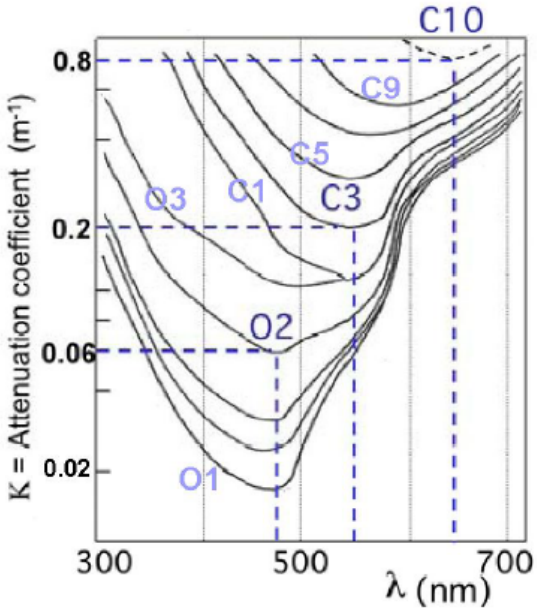

Figure 2.5: Attenuation coefficient of water versus the wavelength of light for different water type [24].

the coastal water types. Fig. 2.5 also shows the relationship between the wavelength of light and $c(\lambda)$. For the ocean water types, the wavelength of about 490nm results in the minimum values of $c(\lambda)$, which means the wavelength of the light source for VLC should be chosen around this value to achieve least attenuation in the ocean water types. It can be seem from Fig. 2.5 that the typical values of $c(\lambda)$ are from about 0.017 m^{-1} for the clearest ocean water types to about 0.8 m^{-1} for the most turbid coastal water types [24].

The primary factors leading to a reduction of light intensity or alteration in the direction of an optical signal underwater are absorption and scattering, respectively. $c(\lambda)$ is the linear combination of absorption coefficient $a(\lambda)$ and scattering coefficient $b(\lambda)$ given as [25]

$$c(\lambda) = a(\lambda) + b(\lambda). \tag{2.12}$$

The value of $a(\lambda)$ and $b(\lambda)$ depends on the biological characteristics of the water and

the wavelength of optical signal λ. Specially, the absorption primarily arises from pure water, chlorophyll-a, as well as humic and fulvic acids. The total absorption in seawater results from a combination of intrinsic absorption caused by inorganic components and absorption from organic substances. As a result, the overall absorption coefficient in seawater can be divided into four distinct factors, which are expressed as [25]

$$a(\lambda) = C_w a_w(\lambda) + C_{phy} a_{phy}(\lambda) + C_g a_g(\lambda) + C_n a_n(\lambda), \tag{2.13}$$

where $a_w(\lambda)$ is absorption due to pure water, $a_{phy}(\lambda)$ is absorption due to phytoplankton, $a_g(\lambda)$ is absorption due to gelbstoff and $a_n(\lambda)$ is absorption due to non-algal material suspensions; and C_w, C_{phy}, C_g and C_n are the corresponding concentrations of inorganic and organic particles.

In open ocean environments where chlorophyll, humic, and fulvic concentrations are typically low, the absorption spectrum is primarily influenced by the attenuation caused by pure water. In such cases, the region of minimum attenuation falls within the range of 400-500 nm, which corresponds to the blue-green region of visible light. However, in coastal regions characterized by higher concentrations of chlorophyll and gelbstoff, the minimum absorption window shifts to a range between 520 and 570 nm, corresponding to the yellow-green region [25].

Scattering in ocean water arises from both organic and inorganic particles suspended within the water. Additionally, variations in temperature, pressure, and salinity can alter the refractive index at optical boundaries, leading to deviations in the light propagation path. For ocean water, the probability of forward scattering is significantly higher than that of backward scattering, where the Mie scattering is the best fitting model to described. The scattering coefficients for large and small particles within ocean water by Mie scattering are given as [26]

$$b_s(\lambda) = 1.151302 \left(\frac{400}{\lambda}\right)^{(1.17)}, \tag{2.14}$$

$$b_l(\lambda) = 0.341074 \left(\frac{400}{\lambda}\right)^{(0.3)}, \tag{2.15}$$

where $b_s(\lambda)$ and $b_l(\lambda)$ are the scattering coefficients for small and large particles, respectively.

2.1.5 Turbulence and Bubbles

Due to the heterogeneity and movement of water bodies, there are always bubbles and turbulence at the surface and in the water. As the light travels in such water, its intensity exhibits strong fluctuations, commonly referred to as scintillation, which deteriorates the performance of VLC [19]. A common indicator used to quantify the fluctuation of light intensity is scintillation index of the received signal, which is expressed as [27]

$$\sigma_I^2 = \frac{\langle I^2 \rangle - \langle I \rangle^2}{\langle I \rangle^2}, \tag{2.16}$$

where I is the received light intensity and $\langle . \rangle$ is the mean operator. A higher value of the scintillation index represents inferior water condition that has more bubbles and stronger turbulence, which leads to a poorer air-water VLC performance.

There are some experimental studies on the impact on the VLC link by different types of air bubble. Substantial obstructing the signal beam is caused by the presence of larger bubbles, resulting in signal fading and potential communication failure. Conversely, smaller bubbles exert a negligible influence on the degradation of link performance [30].

Recent works have studied the impact of turbulence on the light intensity [28] [29]. To characterize the statistical distribution of the underwater turbulence , the lognormal distribution is popularly used. For weak turbulence scenario, the probability density function $f(I)$ of the light intensity is given by [28]

$$f(I) = \frac{1}{I\sigma_I\sqrt{2\pi}} \exp\left(-\frac{(\ln(I/I_0) - \mu)^2}{2\sigma_I^2}\right), \tag{2.17}$$

where σ_I^2 is the scintillation index, I_0 is the mean received light intensity, and μ is the mean logarithmic light intensity. In [50], the depth-dependent factors (e.g., salinity and temperature), which result in the variations of turbulence strength, are explored in the vertical channel. Generally, the turbulence in the water is stronger than in the atmosphere, and in [51], both uplink and downlink between an aerial and an undersea vehicle are modelled, in which a laser beam penetrates through the air-sea turbulence channel. Moreover, laboratory experiments also show that both the surface waves and the depth of the turbulence affect the laser beam centroid drifting and scattering, in which the turbulence near the surface is the primary component [52].

2.1.6 Noises at the Receiver

In this section, the air-to-water VLC that the receiver is placed underwater is mainly considered since the background noise at the underwater environment is more complex and important than that in the air. Most of the noise sources in underwater environment are described as continuous spectrum and Gaussian profile [25].

The underwater receiver is affected by the background noises, dark current noise, thermal noise, and shot noise, which are assumed to follow independent zero-mean Gaussian distributions with variance of σ_{BG}^2, σ_{DC}^2, σ_{TH}^2 and σ_{SS}^2, respectively [24, 31].

Hence, the variance σ_n^2 of the noise term n_i for air-to-water VLC is given by:

$$\sigma_n^2 = \sigma_{\mathrm{BG}}^2 + \sigma_{\mathrm{DC}}^2 + \sigma_{\mathrm{TH}}^2 + \sigma_{\mathrm{SS}}^2. \tag{2.18}$$

The background noise is strongly dependent upon the wavelength of light source and the geographical location. Generally, the noise in the deep ocean is less than that in coastal, especially in harbor, due to human activities [25]. The background noises consist of the solar interference and the blackbody radiation noise caused by biological luminescence, where the former is the main background noise in the euphotic zone of the ocean, and the latter is the principle optical noise source at larger depths [25]. The background noise variance is given by [31]:

$$\sigma_{\mathrm{BG}}^2 = 2q\Re P_{\mathrm{BG}} B, \tag{2.19}$$

$$\Re = \frac{\gamma q \lambda}{hc}, \tag{2.20}$$

$$P_{\mathrm{BG}} = P_{\mathrm{BG\_solar}} + P_{\mathrm{BG\_blackbody}}, \tag{2.21}$$

where the solar background noise $P_{\mathrm{BG\_solar}}$ is [31]

$$P_{\mathrm{BG\_solar}} = A {F_V}^2 B_O T_F W R L_f e^{-c(\lambda)z}, \tag{2.22}$$

and the blackbody radiation background noise $P_{\mathrm{BG\_blackbody}}$ is [31]

$$P_{\mathrm{BG\_blackbody}} = \frac{2hc^2 \alpha \pi {F_V}^2 A T_A T_F B_O}{\lambda^5 [\exp(hc/\lambda k_B T) - 1]}, \tag{2.23}$$

where $\Re$ is the responsivity, γ is the quantum efficiency of the photodetector at the receiver, $q = 1.6 \times 10^{-19}$coulombs is the elementary charge, λ is the wavelength of the light signal, $h = 6.6261 \times 10^{-34}$J is Plank's constant, $c = 2.25257 \times 10^8$m/s is the

speed of light, A is the receiving area of the receiver, F_V is the field of view of the receiver, B_O is the optical filter bandwidth, T_F is the optical filter transmissivity, W is the downwelling irradiance of the sun in watt/m^2, R is the underwater reflectance of downwelling irradiance, L_f is the factor describing the directional dependence of underwater radiance, z is the light propagation distance in the water, and B is the bandwidth of the received light signal, $\alpha = 0.5$ is the radiant absorption factor, $T_A = \exp(-\tau)$ is the transmission in water, $k_B = 1.381 \times 10^{-23}$J/K is the Boltzmann's constant, and T is the temperature of the noise equivalent.

Thermal noise, shot noise, and dark current noise are major noise sources in a photodiode. Thermal noise is generated by the load resistor and its variance is given by [31]:

$$\sigma_{\mathrm{TH}}^2 = \frac{4k_B T_e F B}{R_L}, \tag{2.24}$$

where T_e is the equivalent temperature in K, F is the circuit noise figure, B is the bandwidth of the received light signal and R_L is the load resistance.

Shot noise, also known as quantum noise, arises from the nature of photodetection and its variance is given by [31]:

$$\sigma_{\mathrm{SS}}^2 = 2q\Re P_{\mathrm{RX}} B. \tag{2.25}$$

where P_{RX} is the received light power.

Dark current noise is caused by the constant current that exists when no light is incident on the photodiode and its variance is given by [31]:

$$\sigma_{\mathrm{DC}}^2 = 2qI_{\mathrm{DC}} B, \tag{2.26}$$

where I_{DC} is the dark current of the photodiode and its value depends on the structure of the p-n junction, the doping levels of the material, and the temperature of the

photodiode.

For water-to-air VLC, since the receiver is placed in the air on the UAV, the noise at the receiver is different from that for air-to-water VLC at the background noise term. The background noise for water-to-air VLC is commonly considered as a term in the short noise. Therefore, the variance σ_n^2 of the noise term n_i for water-to-air VLC is given by:

$$\sigma_n^2 = \sigma_{\text{SS}}^2 + \sigma_{\text{DC}}^2 + \sigma_{\text{TH}}^2. \tag{2.27}$$

The shot noise is given by [31]

$$\sigma_{\text{SS}}^2 = 2q\Re P_{\text{RX}} B + 2qI_b B, \tag{2.28}$$

where $q = 1.6 \times 10^{-19}$coulombs is the elementary charge, I_b is the background noise current. The other noises are similar as those for air-to-water VLC.

2.1.7 Modulation Schemes

To enable the transmission of information through light, it is necessary to introduce a systematic variations of light, i.e. modulation, to convey the signal. Subsequently, upon receiving the modulated light, decoding process needs to be done to reconstructs the initial signal.

In most of the current OWC system, OOK is adopted encode the signal as a sequence of light pulses in a binary form. OOK is sometimes describled as amplitude modulation, and it is a special case of amplitude shift keying (ASK) where multiple discrete amplitude levels are employed for the transmission of a digital signal [53].

In OOK modulation, NRZ is the most straightforward encoding method if the bit stream is intended to transmit by merely using the presence or absence of light, where the presence of a carrier (i.e., a constant positive light intensity) during a whole bit

period represents a logic one and the absence of the carrier (i.e., zero light intensity) in a bit period represents a logic zero. This is illustrated in Fig. 2.6 [53].

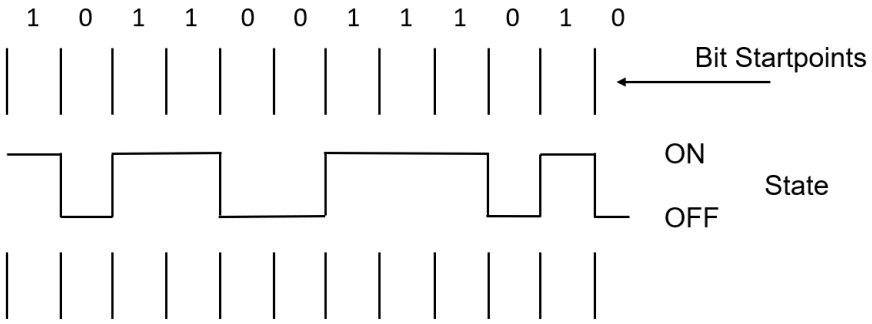

Figure 2.6: NRZ coding illustration [53].

However, the sharp square wave in the figure is the hypothetical pulse. In reality, the transmitting laser or LED cannot response instantly and the output signals have much variations compared to the hypothetical square wave. Moreover, there will be some light emitting during the off state since the responsiveness of the laser or the LED is notably enhanced when it operates just below the threshold level. Therefore, when the signal is received, the receiver has to decide what line state is a "1" bit and what line state is a "0" bit by compare the received light amplitude to a certain amplitude level, and where the bits start and end which depends on the accuracy of the receiver's clock compared with the transmitter's clock. A slight disparity between their timekeeping can impact the synchronization and overall performance of the transmission. To recover the received signal, digital phase locked loop is a simple and economical technique for NRZ coding [53].

In the case of return-to-zero (RZ) coding, the signal reverts to the zero state at the middle of each bit time. As shown in Fig. 2.7 [53], a "1" bit is denoted by an "ON" state for just half of a bit time and return to "0" state for the other half of the time, while a "0" bit is denoted by "0" state for the whole bit period.

In a scenario with limited bandwidth, RZ coding is not the preferred choice. The

main reason is that two distinct line states are required to represent a "1" bit. Consequently, the communication channel must be capable of accommodating a significantly broader analogue bandwidth than what would be necessary for other coding techniques like NRZ. Therefore, RZ is normally used in certain environments, such as in optical fibre, where the bandwidth constraints are not a primary consideration [53].

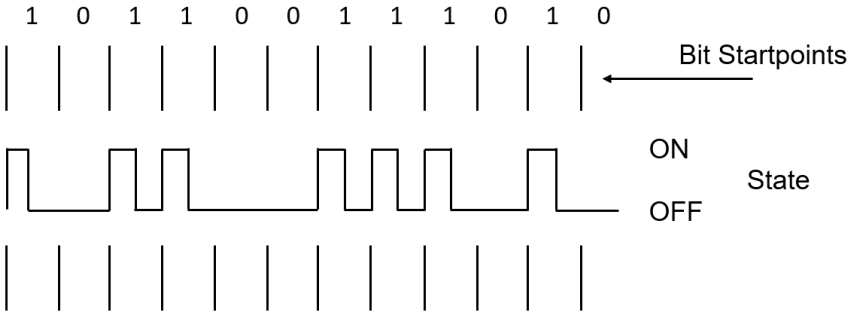

Figure 2.7: RZ coding illustration [53].

To increase the bit rate in a optical link where the maximum signal frequency is limited, multi-state codes are normally used, in which multiple bits are represented by a single line state. Multi-state coding are commonly used in electronic systems where both signal amplitude and phase can be used for distinct line states that representing certain bit combinations. However, in optical communication the phase of the optical signal cannot easily modified. Therefore, to achieve multi-state coding the optical signal amplitude is normally used [53]. Fig. 2.8 shows an example of multi-state coding where four-level coding is used.

Although multi-state coding increases the bit rate compared to NRZ or RZ coding, it requires the transmitter to send several discrete signal levels and the receiver to discriminate these signal levels. Therefore, the cost of the transmitter and the receiver is increased [53].

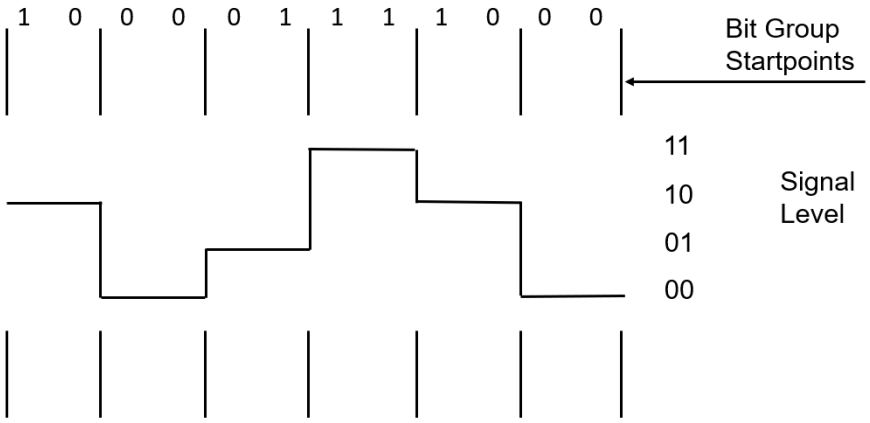

Figure 2.8: Multi-state coding illustration [53].

2.2 Literature Review

2.2.1 Air-to-water Communications

Researchers have recently started to study air-to-water communications without using a relay. Chai et al. [9] developed a MI system where the MI signals were transmitted by an antenna located 2 meters above the water surface and received by a three-component flux gate sensor submerged 35 meters below the water surface. Although error-free transmissions were achieved, the system required a large coil antenna with a cross-sectional area of 4 m^2 and very high transmit power due to large path loss of RF signals in the water. Zhao et al. [16] used a 1064 nm wavelength Nd:YAG laser with a pulse width of 10ns above a 1.2 (L) $\times$ 0.6 (W) $\times$ 0.4 (H) m^3 water tank to generate acoustic waves at a frequency from 1 to 20 Hz in the water. The hydrophone underwater successfully detected the LIA signals, but the transmission distance was within 1 meter and the BER was not discussed.

There are also many recent works studying the air-to-water communication achieved by VLC. In case of LOS, Carver et al. [54] carried out experiments in a swimming

pool using a 140 mW green laser to transmit from 6.5 meters above the water to an ultrasonic sensor array 2.5 meters beneath the water surface and achieved a data rate of 5.03 Mbps with zero BER. However, laser light transmission has a very high directivity and requires the transmitter and receiver to be precisely aligned, which is difficult to realize in practical air-to-water communications.

On the other hand, DLOS VLC are used in air-to-water system that requires a larger light coverage area or the mobility of the transmitter or receiver. In [41], three collinear LEDs were used to increase the VLC underwater coverage area and the received signal strength under turbid water conditions, but whether a transmission was successful or not was determined only by comparing the received light power with a threshold value, without considering the noise or the air-to-water VLC channel effects. Moreover, there was no information about how the LEDs were held above the water in [41], and thus the associated energy consumption was not considered. Kachhadiya and Kashyap [55] tested a two-way VLC link between a glider carrying a transceiver and an underwater transceiver in a swimming pool, where each transmitter employed an array of 16x16 LEDs. They achieved a BER of less than 10^{-4} using OOK modulation with the glider flying within 30 meters above the water and the underwater transceiver being at 2 meters beneath the water surface. However, the water in the swimming pool was clean and steady (i.e., a flat water surface), which is often not the case in realistic air-to-water communication scenarios. [56] investigates the effect of strong ambient light in an air-water VLC link which use a green LED 75 cm above a water tank as the transmitter and a white LED 13 cm above the water surface as the ambient light source. From their experimental results, the APD receiver which is 11 cm depth beneath the water surface reaches the saturation limit under the strong ambient light by the white LED in calm water surface scenario. In wavy water surface scenario, the APD occasionally function outside the saturation region and the variation of air-to-water VLC link gain over time

allows opportunities for communication, which suggests that the presence of a wavy water surface can mitigate the impact of ambient light. However, only communication possibility is discussed and there is not an actual air-water VLC link establishment in this work.

2.2.2 Water-to-air Communications

In [15], TARF is designed to make the air-water interface itself to become a medium for water-to-air communication. TARF was realized by deploying a high-frequency radar 20 to 40 cm above water to decode the vibrations on the water surface caused by sonar signals sent from an acoustic transmitter placed 5 to 70 cm underwater in a water tank. Sonar signals sent by acoustic transmitter travel as pressure waves, which representing 0 and 1 bits according to preset frequency, will cause ripples on the water surface. To detect the ripples, the radar sends a radio signal towards the water surface which reflects off the ripples and rebounds back to the radar. The returned signal has a marginally modulated angle because of the vibration of water surface, and the vibration frequency of this signal's angle can then be read and represents its corresponding data bit. Similarly, an experimental study is done by using a laser Doppler interferometer as a sensor 1.6 m above the water to detect the oscillatory motion of water surface caused by the acoustic signals sent from an acoustic transmitter 2 m underwater [57]. In [58], a two-way air-water communication is achieved in a water tank by using thermoacoustic effect for air-to-water link and microwave vibration measurement technology for water-to-air link. For the water-to-air link, the modulated ultrasonic signals are transmitted from an underwater transducer and an airborne radar is used to measure the surface displacement on the air-water interface. However, these water-to-air systems does not simultaneously support air-to-water transmissions and thus requires another approach to setup the air-to-water link. Also, their experimental environment is in the swimming

pool or water tank, but once applied in ocean environment where the water wave amplitude is much higher, the decoding of the signals from the air-water interface will be much more challenging.

For LOS VLC, Sangeetha et al. [59] used a 635 nm laser diode with an output power of 4.8 mW (placed beneath a glass water tank) to transmit to a silicon photo detector (located 0.5 meter above the water surface), where the 1.81 (L) $\times$ 0.3 (W) $\times$ 0.52 (H) m^3 glass tank was filled with water of 0.3 m depth, and achieved a BER of 10^{-3} at a baud rate of up to 110 Kbps.

For recent related works on DLOS VLC, [60] experimentally study a pre-aligned DLOS laser-based water-to-air VLC system in a canal of the Red Sea, where the white-light divergent laser diode as the transmitter is placed 1.5 m below the water and the receiver in the air is 1 m above the water surface, and achieved a data rate of 87 Mbit/s for over 50 min. However, even by using divergent laser to establish a VLC link of DLOS , this system needs to be pre-aligned to work and perfectly aligned to reach maximum data rate.

In [61], a water-to-air VLC link is experimentally studed in a water tank by using a green LED at depth 11 cm under the water surface to transmit optical signals to a receiver 54 cm above the water surface. A BER of 10^{-4} to 10^{-2} is achieved depending on the different horizontal positions of the receiver. [62] establishes a water-to-air VLC link in a laboratory water tank environment placing the LED transmitter 0.2 m from the bottom of the 3 (L) $\times$ 1 (W) $\times$ 0.6 (H) m^3 water tank filled with 0.3 m depth of water and the avalanche photodiode (APD) receiver is 2 m above the water surface, and studies the impact of different types of water waves. From their Monte Carlo simulations and experimental findings, the small-scale waves primarily impact the energy distribution within the light spot on the receiving plane and the frequency of variations in link gain. In contrast, large-scale waves predominantly influence the

coverage of the light spot. [35] setups an experimental water-to-air VLC link using optical camera as the receiver instead of conventional APD. The LED transmitter is placed under a 50 (L) $\times$ 23 (W) $\times$ 28 (H) cm^3 water tank and the complementary metal-oxide semiconductor based optical camera is placed 40 cm above the water. A data rate of 16.56 Kbit/s is achieved with BER less than 10^{-3}. However, these works are lack of a mathematical water surface model and the complexity of the water wave and transmission distance in the water tank environment is limited. In [63], a prototype of the software-defined VLC modem is created and experimental assessment is done both in a water tank and in an ocean environment for bi-directional air-water VLC link. BER performance is compared among different modulation schemes in the laboratory water tank environment. For ocean experiments, two proposed prototypes of software-defined VLC modem are used in a coastal ocean area and achieve a data rate of 1 Mbit/s using OFDM modulation scheme. However, in their ocean experiments, the VLC modems are fixed 1 m away from each other, which is usually not a sufficient transmission distance for realistic air-water applications. [33] proposed a concatenated Reed Solomon-Low Density Parity Check coding is to improve the reliability of a water-to-air VLC link. This coding scheme includes error-correcting code and erasure-correcting code, and experimental study the performance of the proposed coding in a laboratory environment by adopting a green LED as the transmitter at depth 12 cm beneath the water surface to transmit to an APD receiver placed at height of 72 cm above the water surface. With sampling rate of 50 MSa/s and symbol rate of 10 MSym/s, by increasing the code length and lowering the code rate, the proposed coding scheme corrects both bit error and frame loss and provides larger correct frame ratio to improves the the water-to-air VLC link performance. However, the water surface model is not considered mathematically, and the performance of the proposed coding scheme is only compared with the same coding structure with variation of parameters

settings but not other benchmark coding schemes.

2.2.3 UAV-assisted Air-water Communications

Unmanned autonomous vehicles, such as aerial UAVs and underwater autonomous underwater vehicles (AUVs), offer a range of advantages, including high mobility, rapid deployment and flexible reconfiguration for communication across the air-water interface. These qualities make them ideal terminal endpoints for establishing direct cross-boundary VLC links [19]. However, the stability of the UAVs and AUVs faces the challenge from the turbulence in the air or water, which may lead to variations of position or light propagation direction. Therefore, utilizing UAVs or AUVs for air-water VLC is more challenging in robustness than placing the transmitter and receiver in a fixed location.

Waterproof UAVs can float on the water surface to communication with underwater nodes. In this case, the UAV either act as a relay between the underwater transceiver and the transceiver hovering in the air or on the shore, or direct tranmission between the UAV and the underwater transceiver. However, the floating UAV can be vulnerable to the dynamic environmental effects such as drifts, currents or surface waves [63]. In addition, direct acoustic transmission is more reliable in this case since it does not need to transmit through the air-water boundary and does not have the coverage issue in VLC. Therefore, in this thesis, the UAV is considered to be hovering above water to assist the air-water VLC communications.

In many related works, UAV is considered in the air-water VLC model [33,36,61–64]. However, in these works the characteristics of UAV, such as the mobility, stability or energy consumption, are not analysed in the system model, and in the experiments both the transmitters and the receivers are placed in a fixed position instead of using an UAV. In [65], a tracking procedure is proposed to enhance the reliability and robustness

of a two-way air-water laser-based VLC link between an underwater AUV and an aerial UAV in a triple-hop network. In this approach, the UAV continuously emits brief but high-energy pulses to locate and monitor the AUV by measuring the reflections of these pulses. Subsequently, a gimbal tracker mounted on the UAV sweeps across the AUV's surface to locate its optical lens and align the laser link. By adopting the proposed tracking procedure, the outage probability is achieved to be less than 10^{-4} and the BER is less than 10^{-3} at SNR of 40 dB. However, in their channel model between the UAV and the AUV, the impact of the air-water interface, such as reflection and refraction, is not considered but the path loss and turbulence are considered for a whole link for both air and water. In [66], an airborne node is employed to assist the AUVs in localizing themselves by using an air-to-water VLC link. The stationary airborne node such as an hovering UAV sends VLC signals providing its GPS coordinate and height to the AUVs which are moving in a certain depth. Since the AUVs knows their depth by the pressure sensor, they can calculate their global coordinates by the different received light intensities from several air-to-water VLC transmissions. However, this work simulates a flat water surface where the impact of the water wave is not considered, which the wavy water surface should have a significant effect on the received light intensity in reality.

2.2.4 Energy Consumption

To establish a sustainable, long-term cross-boundary monitoring network and minimize the impact on the marine ecological environment, it is crucial to place a stronger emphasis on addressing the energy-related challenges. Although the performance of air-water VLC is notably influenced by the complex and dynamic of the air-water interface, it encounters substantially lower signal attenuation and results in lower energy consumption, as compared to other approaches such as RF, EM and MI [19].

An amorphous silicon thin-film solar cell is proposed in [67] for VLC photoreceiver, and a prototype that consists of a solar panel and receiver circuits is designed, which can detect faint light signals as low as 1 $\mu W/cm^2$. In combination with a white-light laser, they achieved a data rate of 1 Mb/s for an underwater link of 2.4 m in a turbid water pool with background light illumination intensity of 100 mW/cm2. Due to the four solar cells in the prototype, the energy harvested exceeded the requirements to power the VLC receiver circuits. However, in air-water cross-boundary VLC, the energy consumption of the transmitter and the aerial platform such as UAV that carries the transmission terminal generally play a much more important role in the total energy consumption of the VLC system.

In [68], a low-cost passive relay is used on the water surface to convert the light energy from a laser transmitter in the air into ultrasound energy to generate photoacoustic wave. By using this approach, the single laser pulse energy is reduced to 27 μJ compared to tens of joules for using laser to transmit the whole air-water link. However, the communication delay is large due to the low velocity of sound, the air link between the laser transmitter and the passive relay faces severe misalignment issue, and a relay is required in this system.

Chapter 3

Energy Consumption Minimization of Air-to-Water VLC

3.1 Overview

In this charpter, an air-to-water VLC system where an UAV carrying an LED transmitter hovers above the water and sends VLC signals to an underwater receiver is considered. Since light in the blue-green wavelength range between 450-570 nm has the minimum absorption and scattering coefficients in water among all optical wavelength ranges [69], an LED transmitter that has a dominant wavelength in this range will be considered. The underwater receiver is located no more than 20 meters beneath the water surface.

Although the UAV may locate the underwater receiver after successfully establishing a VLC link, the position of the receiver may change continuously due to the water movements and the water surface changes continuously with time. Therefore, reducing the beam angle of the LED or equipping another laser transmitter to communicate after locating the underwater receiver requires frequent updates of the underwater re-

ceiver's position and results in high complexity and high overhead for the system. In this thesis, the LED transmitter with a fixed beam angle is considered.

Using a laser transmitter with beam tracking may increase the transmission rate, but the alignment issue is challenging in the considered VLC system model. Due to the rapid and unpredictable changes in the light spot location at the underwater receiver plane, common beam tracking methods such as picture processing using an image sensor and position sensor detector (PSD) are not effective when the light signal passes through the time-varying wavy water surface [34]. The underwater receiver may include a photodiode array to obtain a larger detection area, but this will also compromise the location accuracy [34]. In the considered VLC system model, the water surface is time-varying and the underwater receiver is drifted away by the water current to a random position within a range. Therefore, the LED transmitter instead of a laser transmitter is considered as it generally has a wider beam angle and results in an acceptable coverage area.

3.2 Air-to-Water VLC System Model

3.2.1 Water Surface Model

The cross section of an air-to-water communication environment at a given time instant is plotted in the (x, y) plane in Fig. 3.1. The water wave is considered to be a deep water wave, where the wavelength of the water surface wave is smaller than the water depth. According to Stokes's third-order theory [21], the water surface elevation can be expressed as follows:

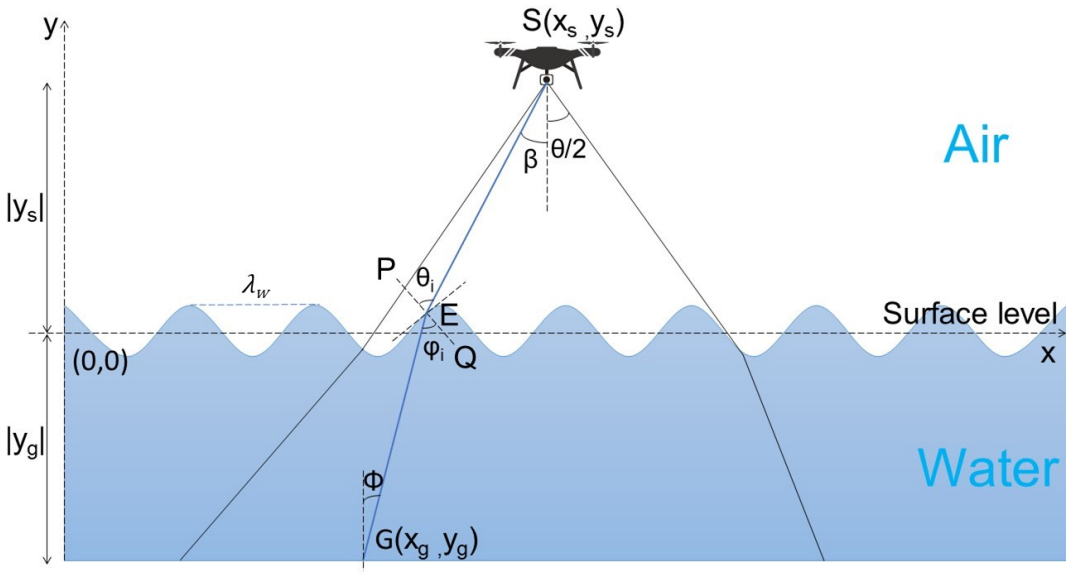

Figure 3.1: A cross section of the air-water interface.

$$
\begin{aligned}
f(x,t) =& \alpha \left\{ \left[1 - \frac{1}{16}(k\alpha)^2 \right] \cos(kx - \omega t) \right. \\
&+ \frac{1}{2}(k\alpha) \cos\left[2(kx - \omega t)\right] \\
&\left. + \frac{3}{8}(k\alpha)^2 \cos\left[3(kx - \omega t)\right] \right\} + O\left[(k\alpha)^4\right], \qquad (3.1) \\
k =& \frac{2\pi}{\lambda_w}, \qquad (3.1a) \\
\omega =& k \left[1 + \frac{1}{2}(k\alpha)^2 \right] \sqrt{\frac{g}{k} + O\left((k\alpha)^4\right)}, \qquad (3.1b)
\end{aligned}
$$

where x is the horizontal coordinate of a point on the water surface, t is time, ω is the angular frequency of the water wave, α is the first-order wave amplitude, k is the angular wavenumber, $k\alpha$ is the wave steepness, $O((k\alpha)^4)$ is the sum of least significant terms, λ_w denotes the wavelength of water waves, and g is the gravitational acceleration.

The time period T_w of the water wave is given by:

$$T_w = \frac{2\pi}{\omega}. \tag{3.2}$$

3.2.2 Light Propagation Path

For analytical tractability, it is assumed that the LED transmitter points downward vertically and the underwater receiver points upward vertically. Denote the positions of the LED transmitter and the underwater receiver by S and G, respectively, then the coordinates of S and G in the (x, y) plane are (x_s, y_s) and (x_g, y_g), respectively. The UAV knows the default position of the underwater receiver at (x_s, y_g) and hovers straight above it, but the underwater receiver may be drifted away from its default position by the water current. It is assumed that the underwater receiver is kept within a radius of x_0 from its default position at the water depth $|y_g|$ by a mooring cable [70]. In [71], an underwater node is moored by a cable to the seafloor and the underwater node movement due to the ocean current is modelled by the Gaussian radial basis function. In this thesis, the light signal needs to cover all possible underwater receiver positions in the circular area at all times for the VLC link regardless how the underwater receiver position is distributed in this area.

The incident point of the light propagation path on the water surface is denoted by E with coordinates (x_e, y_e). According to Snell's law [49], the relationship between the incident angle θ_{i} and the refraction angle φ_{i} is given by:

$$n_a \sin(\theta_{\mathrm{i}}) = n_w \sin(\varphi_{\mathrm{i}}), \tag{3.3}$$

where $n_a = 1$ and $n_w = 1.333$ are the refractive index of air and water, respectively.

Let m_{PQ} and m_{SE} be the slope of line $\overline{\mathrm{PQ}}$ and $\overline{\mathrm{SE}}$, respectively. They are given by

$$m_{\mathrm{PQ}} = -1/\left[\frac{\partial f\left(x_e, t\right)}{\partial x_e}\right], \tag{3.4}$$

$$m_{\mathrm{SE}} = \frac{y_s - f\left(x_e, t\right)}{x_s - x_e}. \tag{3.5}$$

The relationship between θ_{i}, m_{PQ} and m_{SE} is:

$$\tan\theta_{\mathrm{i}} = \left|\frac{m_{\mathrm{PQ}} - m_{\mathrm{SE}}}{1 + m_{\mathrm{PQ}} m_{\mathrm{SE}}}\right|. \tag{3.6}$$

Substituting (3.4) and (3.5) into (3.6), the angle θ_{i} is given by

$$\theta_{\mathrm{i}} = \tan^{-1}\left|\frac{\left[y_s - f\left(x_e, t\right)\right]\frac{\partial f(x_e,t)}{\partial x_e} + \left(x_s - x_e\right)}{\left(x_s - x_e\right)\frac{\partial f(x_e,t)}{\partial x_e} - y_s + f\left(x_e, t\right)}\right|. \tag{3.7}$$

Similarly, the angle φ_{i} can be calculated by

$$\varphi_{\mathrm{i}} = \tan^{-1}\left|\frac{\left[y_g - f\left(x_e, t\right)\right]\frac{\partial f(x_e,t)}{\partial x_e} + \left(x_g - x_e\right)}{\left(x_g - x_e\right)\frac{\partial f(x_e,t)}{\partial x_e} - y_g + f\left(x_e, t\right)\Big)}\right|. \tag{3.8}$$

Substituting (3.7) and (3.8) into (3.3), (3.3) can be solved for x_e and then $y_e = f\left(x_e, t\right)$ can be obtained based on (3.1). When there are several solutions of x_e from solving (3.3), the proper solution is selected by checking whether or not the resulting slopes of lines $\overline{\mathrm{SE}}$ and $\overline{\mathrm{EG}}$ and the normal line at the incident point E are reasonable for light refraction. Substituting the proper x_e into (3.7) and (3.8), θ_{i} and φ_{i} can be obtained.

The transmission distances above the water and underwater, the angle β between the optical axis of the LED and the light propagation direction above the water, as well as the angle ϕ between the underwater light propagation direction and the optical

axis of the receiver, can be calculated respectively by:

$$|\mathrm{SE}| = \sqrt{(x_e - x_s)^2 + (y_e - y_s)^2}, \tag{3.9}$$

$$|\mathrm{EG}| = \sqrt{(x_e - x_g)^2 + (y_e - y_g)^2}, \tag{3.10}$$

$$\beta = \tan^{-1}\left|\frac{x_e - x_s}{y_e - y_s}\right|, \tag{3.11}$$

$$\phi = \tan^{-1}\left|\frac{x_e - x_g}{y_e - y_g}\right|. \tag{3.12}$$

Other cross sections of the air-to-water communication environment can be obtained by rotating the cross section in Fig. 3.1 horizontally for an angle in the range from 0 to 180 degrees [41]. The water surface elevation function in the cross section that is rotated around the line of $x = x_s$ from the cross section containing $f(x,t)$ by an angle of δ is given by:

$$f(x',t) = f[x\cos(\delta), t], \tag{3.13}$$

where $x' = x\cos(\delta)$. The light propagation path in each new cross section can be obtained in a way similar to the above.

3.2.3 Received Light Power

Without loss of generality, it is assumed that the LED transmitter adopts the OOK-NRZ modulation, where the presence of a carrier (i.e., a constant positive light intensity) during a whole bit period represents a logic one and the absence of the carrier (i.e., zero light intensity) in a bit period represents a logic zero [53].

The transmitted information bits are recovered by the receiver using a matched filter for direct-detection [47]. The resulting electrical signal sampled at the output of the matched filter can be expressed as [48]:

$$Y_i = \eta I X_i + n_i, \tag{3.14}$$

where η is the optical-to-electrical conversion coefficient, I is the light intensity of the received signal, $X_i \in \{0, 1\}$ is the ith information bit, and n_i is the AWGN in the ith bit period. The AWGN has a zero mean and variance σ_n^2. According to [48], η is given by:

$$\eta = \frac{\gamma T_b q \lambda}{hv}, \tag{3.15}$$

where γ is the quantum efficiency of the photodetector at the receiver, T_b is the bit interval, $q = 1.6 \times 10^{-19}$coulombs is the elementary charge, $h = 6.6261 \times 10^{-34}$J is Plank's constant, $v = 2.25257 \times 10^8$m/s is the speed of light in the water, and λ is the wavelength of the light signal in the water.

In addition to refraction, the water surface also affects the transmittance due to reflection depending on the incident angle. Letting τ denote the transmittance, it is calculated according to Fresnel's equation [49] by:

$$\tau = 1 - \frac{\left|\frac{n_a cos\theta_{\mathrm{i}} - n_w cos\varphi_{\mathrm{i}}}{n_a cos\theta_{\mathrm{i}} + n_w cos\varphi_{\mathrm{i}}}\right|^2 + \left|\frac{n_a cos\varphi_{\mathrm{i}} - n_w cos\theta_{\mathrm{i}}}{n_a cos\varphi_{\mathrm{i}} + n_w cos\theta_{\mathrm{i}}}\right|^2}{2}. \tag{3.16}$$

Turbulence may cause the fluctuation of light intensity, known as scintillation, at the underwater receiver [72]. The scintillation index is usually used to quantify the scintillation and it is mainly affected by the light propagation distance and the dissipation rate of mean squared temperature [72]. In this VLC system, a VLC link operating in a water volume characterized by weak turbulence is considered, where the underwater receiver is located no more than 20 meters beneath the water surface and the dissipation rate of mean squared temperature does not exceed $1 \times 10^{-8}\mathrm{K}^2/\mathrm{s}$, a typical

value observed in the Pacific Equatorial Undercurrent region [73]. As shown in Fig. 1 of [72], the scintillation index is nearly zero for any dissipation rate of mean squared temperature below $1 \times 10^{-8}\mathrm{K}^2/\mathrm{s}$ and light propagation distances of no more than 20 meters beneath the water surface. Therefore, the effect of turbulence is considered to be neglectable in this system.

With light propagating for a distance $\overline{\mathrm{SE}}$ in the air, passing through the air-water interface with transmittance τ, and propagating for a distance $\overline{\mathrm{EG}}$ underwater, we can obtain the light intensity I at the underwater receiver according to Beer's law [41] [49] as follows:

$$\begin{aligned} I &= \frac{2\pi}{\theta} \times \frac{P_{\mathrm{TX}}}{4\pi|\mathrm{SE}|^2} \times \tau \times e^{-k_w|\mathrm{EG}|} \\ &= \frac{P_{\mathrm{TX}}\tau e^{-k_w|\mathrm{EG}|}}{2\theta|\mathrm{SE}|^2}, \end{aligned} \tag{3.17}$$

where P_{TX} is the LED transmit power and k_w is the attenuation coefficient of water that depends on the biological factors of water as well as the light wavelength. In a given underwater environment, k_w may vary with the depth of the observation point underwater. However, according to the measurement results in [74], the change of k_w is negligible when it is measured at depths in the range from 10 to 30 meters (i.e., the euphotic zone of the ocean), which is the range of depths at which the target underwater receiver is deployed, hence k_w is considered as a constant for simplicity.

The received power P_{RX} at the underwater receiver is then given by:

$$P_{\mathrm{RX}} = IAcos\left(\phi\right), \tag{3.18}$$

where A is the receiving area of the underwater receiver.

3.2.4 Underwater Received SNR

The underwater receiver is affected by the background noises, dark current noise, thermal noise, and shot noise, which are assumed to follow independent zero-mean Gaussian distributions with variance of σ^2_{BG}, σ^2_{DC}, σ^2_{TH} and σ^2_{SS}, respectively [24, 31]. Hence, the variance σ^2_n of the noise term n_i is given by:

$$\sigma^2_n = \sigma^2_{\mathrm{BG}} + \sigma^2_{\mathrm{DC}} + \sigma^2_{\mathrm{TH}} + \sigma^2_{\mathrm{SS}}. \tag{3.19}$$

The background noises consist of the solar interference and the blackbody radiation noise caused by biological luminescence, where the former is the main background noise in the euphotic zone of the ocean, and the latter is the principle optical noise source at larger depths [25]. In the VLC system where the underwater receiver is deployed in the euphotic zone, the blackbody radiation noise is negligible [75]. Thus, the background noise variance is given by [31]:

$$\sigma^2_{\mathrm{BG}} = 2q\Re A {F_V}^2 B_O T_F W R L_f e^{-k_w|y_g|} B, \tag{3.20}$$

$$\Re = \frac{\gamma q \lambda}{hc}, \tag{3.21}$$

where $\Re$ is the responsivity, F_V is the field of view of the receiver, B_O is the optical filter bandwidth, T_F is the optical filter transmissivity, W is the downwelling irradiance of the sun in watt/m^2, R is the underwater reflectance of downwelling irradiance, L_f is the factor describing the directional dependence of underwater radiance, and B is the bandwidth of the received light signal.

Thermal noise, shot noise, and dark current noise are major noise sources in a photodiode. Thermal noise is generated by the load resistor and its variance is given

by [31]:

$$\sigma_{\mathrm{TH}}^2 = \frac{4k_B T_e F B}{R_L}, \tag{3.22}$$

where $k_B = 1.381 \times 10^{-23}$J/K is the Boltzmann's constant, T_e is the equivalent temperature in K, F is the circuit noise figure and R_L is the load resistance.

Shot noise, also known as quantum noise, arises from the nature of photodetection and its variance is given by [31]:

$$\sigma_{\mathrm{SS}}^2 = 2q\Re P_{\mathrm{RX}} B. \tag{3.23}$$

Dark current noise is caused by the constant current that exists when no light is incident on the photodiode and its variance is given by [31]:

$$\sigma_{\mathrm{DC}}^2 = 2qI_{\mathrm{DC}} B, \tag{3.24}$$

where I_{DC} is the dark current of the photodiode and its value depends on the structure of the p-n junction, the doping levels of the material, and the temperature of the photodiode.

The average SNR at the underwater VLC receiver is expressed as [76]:

$$\begin{aligned} \rho &= \frac{\Re^2 P_{\mathrm{RX}}^2}{\sigma_n^2} \\ &= \frac{\Re^2 I^2 A^2 cos^2(\phi)}{\sigma_{\mathrm{BG}}^2 + \sigma_{\mathrm{DC}}^2 + \sigma_{\mathrm{TH}}^2 + \sigma_{\mathrm{SS}}^2}. \end{aligned} \tag{3.25}$$

3.2.5 Channel Capacity

For OOK-NRZ with direct detection at the receiver, the channel capacity in bit/pulse is given by [48]:

$$C'_{\text{OOK}} = \frac{\rho}{2} log_2(e) - \frac{e^{\frac{-\rho}{4}}}{\sqrt{2\pi}} \int e^{\frac{-t^2}{2}} \cosh\left(t\sqrt{\frac{\rho}{2}}\right) log_2\left[\cosh\left(t\sqrt{\frac{\rho}{2}}\right)\right] dt. \tag{3.26}$$

Since the OOK-NRZ pulse rate is $1/T_b$ pulse/s, the channel capacity in bit/s is then given by:

$$C_{\text{OOK}} = \frac{1}{T_b} C'_{\text{OOK}}. \tag{3.27}$$

3.3 Problem Formulation

3.3.1 The Coverage of Light Signal

Let β_{rt} denote the angle between the optical axis of the LED and the light propagation direction above the water in the cross section that contains $f[x\cos(\delta), t]$, where $\delta \in [0, \pi]$ and $t \in [0, T_w]$, and let θ denote the angular beamwidth of the LED. If $\max_{\delta,t}\{\beta_{rt}\} \leq \frac{\theta}{2}$, then the underwater receiver location $G(x_g, y_g)$ is in the light coverage at all times. Otherwise, in some cross sections, the light propagation path is not inside the LED beam and the underwater receiver location may be outside the light coverage.

3.3.2 BER Requirement for VLC Transmission

For OOK-NRZ under the impact of zero-mean independent Gaussian noise, the relationship between the BER and the received SNR is given by [76]:

$$BER = \frac{1}{2}\,\mathrm{erfc}\left(\frac{1}{2\sqrt{2}}\sqrt{\rho}\right), \tag{3.28}$$

where erfc(.) is the complementary error function. Hence, the required SNR for achieving a target BER is given by:

$$\rho_{\mathrm{req}} = 8\left[\mathrm{erfc}^{-1}\left(2BER_{\mathrm{req}}\right)\right]^2, \tag{3.29}$$

where $\mathrm{erfc}^{-1}(.)$ is the inverse complementary error function, and BER_{req} is the required target BER.

3.3.3 Energy Consumption Minimization

The objective is to minimize the UAV's total energy consumption, which consists of the power used for VLC by the LED and the propulsion power of the UAV when hovering above the water, by optimizing the transmit power of the LED under the following constraints: the underwater receiver is in the LED's light coverage at all times, i.e., $\max_{\delta,t}\{\beta_{rt}\} \leq \frac{\theta}{2}$; and the average SNR at the underwater receiver is above the required SNR ρ_{req} for a given BER, i.e., $\rho \geq \rho_{\mathrm{req}}$. Note that the average SNR at the underwater receiver calculated from (3.25) does not consider the light coverage, and if the light coverage is not met, the resulting SNR value is invalid and the communication fails.

Let D denote the total amount of data (in bits) that needs to be transmitted from the LED to the underwater receiver. With the OOK-NRZ channel capacity C_{OOK} (bit/s), the transmission time t_{TX} (s) required for transmitting D bits of data to the

underwater receiver is given by::

$$t_{\mathrm{TX}} = D/C_{\mathrm{OOK}}. \tag{3.30}$$

Let η_p denote the LED's transmission power conversion efficiency, which may change with the transmit power of the LED and is usually given in the LED product specification. The power dissipation of the LED for data transmission is then P_{TX}/η_p. Thus, the total energy consumption of the UAV during the data transmission time is given by:

$$\begin{aligned} E_{\mathrm{UAV}} &= \left(P_{\mathrm{UAV}} + \frac{P_{\mathrm{TX}}}{\eta_p}\right) t_{\mathrm{TX}} \\ &= \frac{\left(P_{\mathrm{UAV}} + \frac{P_{\mathrm{TX}}}{\eta_p}\right) D}{C_{\mathrm{OOK}}}, \end{aligned} \tag{3.31}$$

where P_{UAV} denotes the propulsion power of the UAV.

Therefore, the UAV energy consumption minimization problem is formulated as follows:

$$\min_{P_{\mathrm{TX}}} E_{\mathrm{UAV}}, \tag{3.32}$$

$$\text{s.t. } \max_{\delta,t}\{\beta_{rt}\} \leq \frac{\theta}{2}, \tag{3.32a}$$

$$\rho \geq \rho_{\mathrm{req}}, \tag{3.32b}$$

$$P_{\min} \leq P_{\mathrm{TX}} \leq P_{\max}, \tag{3.32c}$$

where $P_{\min}$ and $P_{\max}$ denote the minimum and maximum transmit power of the LED, respectively. Their values can be obtained from the LED product specification, e.g., [77].

3.4 Problem Solving

The incident point (x_e, y_e) of the light propagation path on the water surface cannot be obtained from (3.3) analytically because it returns several solutions and the proper solution needs to be identified by checking whether or not each solution is reasonable for light refraction. Hence, a SQP-based algorithm (Algorithm 1) is devised to numerically solve the optimization problem (3.32).

3.4.1 Discrete Spatial-Temporal Environment of Air-to-Water VLC

In Algorithm 1, lines 1-14 firstly analyse the light propagation path from the LED to the underwater receiver and obtain x_e for the incident point E by using (3.1), (3.3)–(3.8) and (3.13), then calculate |SE|, |EG|, β and ϕ using (3.9)–(3.12) for all the cross sections that rotate around the line of $x = x_s$ from 0° to 180° with an increment step size of $\Delta\delta$, each time instant within a time period T_w of the water wave with an increment step size of Δt, and all possible underwater receiver positions at depth $|y_g|$ with x_g increasing from $x_s - x_0$ to $x_s + x_0$ with a step size of Δx_0, where x_0 denotes the longest distance that the underwater VLC receiver may move away from its default location (x_s, y_g). The above 'While' loops construct a discrete spatial-temporal environment for problem (3.32). This is because both the received SNR ρ in the objective function (3.31) and constraint (3.32b) and β_{rt} in constraint (3.32a) depend on the light propagation path that may vary in space and time. Line 15 calculates the required SNR ρ_{req} using (3.29).

3.4.2 SQP-based Algorithm for Optimizing LED Transmit Power

There are many algorithms that can be used to find the optimal LED transmit power, including metaheuristic algorithms such as the genetic algorithm and the particle

swarm optimization algorithm and iterative algorithms such as the SQP algorithm. In this work, we choose the SQP algorithm because it is of a lower complexity than a metaheuristic algorithm for solving our minimization problem. It can be utilized through MATLAB minimization function 'fmincon'. Other iterative algorithms, such as active-set algorithm, are also appropriate for solving this minimization problem. In Algorithm 1, lines 16-24 construct the objective function $E_{\mathrm{UAV}}(P_{\mathrm{TX}})$ using (3.31) under constraints (3.32a) and (3.32b). Line 25 calls the minimization function 'fmincon' to obtain the optimized transmit power P_{opt} that minimizes the objective function $E_{\mathrm{UAV}}(P_{\mathrm{TX}})$ under constraint (3.32c) by using the SQP algorithm. Algorithm 1 runs off-line before the UAV is dispatched.

3.5 Results and Discussion

In this section, the simulation results are presented to evaluate the performance of the proposed algorithm. In this simulation, the UAV DJI Phantom 4 RTK is chosen, which has a take-off weight of 1391g, battery capacity of 89.2 Wh and propulsion power of 178.4 W according to its specification [78]. Because blue-green light attenuates the least while propagating underwater, blue-green light LED LedEngin's LZ4-00B215 which has a dominant wavelength of 465nm in the air [77] and a wavelength of $(n_a/n_w)\times 465\text{nm} = 349\text{nm}$ in water [49] is considered in the simulation, and ten LZ4-00B215 LEDs in an array are arranged as the transmitter. It is assumed that the power consumption of carrying the LEDs has been included in P_{UAV}.

The values of system parameters used in the simulation are listed in Table 3.1, where most of the parameter values are set following [41], [31]. For instance, the depth of underwater receiver is considered to be in the range from 10 to 15 meters, and the attenuation coefficient of water is considered to be from 0.25 m^{-1} to 0.45 m^{-1}.

Algorithm 1 UAV energy consumption minimization

Input: $P_{\min}, P_{\max}, BER_{\text{req}}, T_w, \theta, x_s, x_0$

Output: P_{opt}

$\delta \Leftarrow 0$;
while $\delta \leq 180^\circ$ **do**
  $t \Leftarrow 0$;
  while $t \leq T_w$ **do**
    $x_g \Leftarrow x_s - x_0$;
    while $x_g \leq x_s + x_0$ **do**
      Calculate x_e using (3.1), (3.3)-(3.8), and (3.13);
      Calculate $\beta(\delta, t, x_g)$, $|\text{SE}|(\delta, t, x_g)$, $|\text{EG}|(\delta, t, x_g)$, $\phi(\delta, t, x_g)$ using (3.9)-(3.12);
      $x_g \Leftarrow x_g + \Delta x_0$;
    end while
    $t \Leftarrow t + \Delta t$;
  end while
  $\delta \Leftarrow \delta + \Delta\delta$;
end while
Calculate ρ_{req} using (3.29);
function $E_{\text{UAV}}(P_{\text{TX}})$
  for all δ, t, x_g **do**
    Calculate ρ using (3.25);
    if $\beta(\delta, t, x_g) \leq \theta/2$ and $\rho(\delta, t, x_g) \geq \rho_{\text{req}}$ **then**
      Calculate $E_{\text{UAV}}(P_{\text{TX}}, \delta, t, x_g)$ using (3.31);
    end if
  end for
  $E_{\text{UAV}}(P_{\text{TX}}) \Leftarrow \underset{\delta,t,x_g}{\text{mean}}\left[E_{\text{UAV}}(P_{\text{TX}}, \delta, t, x_g)\right]$;
end function
$P_{\text{opt}} \Leftarrow \text{fmincon}\left[E_{\text{UAV}}(P_{\text{TX}}), P_{\text{TX}}, P_{\min}, P_{\max}, \text{SQP}\right]$;

Table 3.2 shows the values of P_{TX} for ten LZ4-00B215 LEDs and the corresponding η_p values according to the LZ4-00B215 specification [77].

Fig. 3.2 shows the optimized LED transmit power obtained by Algorithm 1 versus the depth of underwater receiver as well as the attenuation coefficient of water, where the incremental step sizes in Algorithm 1 are set as $\Delta\delta = 10°$, $\Delta t = 0.1$s and $\Delta x_0 = 0.2$m. From Fig. 3.2, we can see that the optimized LED transmit power increases with the depth of underwater receiver for a given attenuation coefficient of water and increases with the attenuation coefficient of water for a given depth of underwater receiver. The highest optimized transmit power of 45.7 Watts is required for the worst scenario of $|y_g| = 15$m and $k_w = 0.45\mathrm{m}^{-1}$.

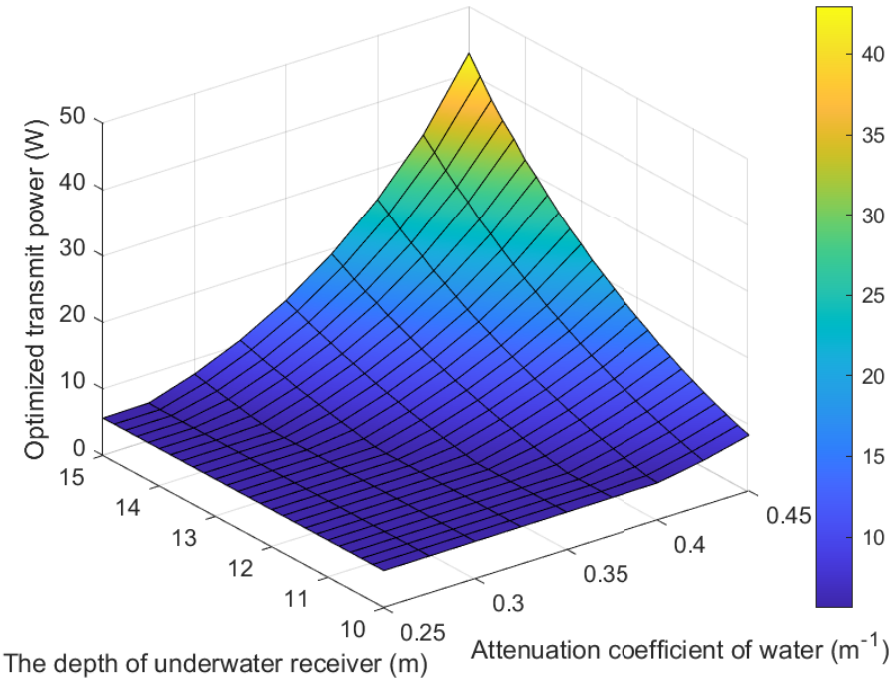

Figure 3.2: Optimized transmit power versus the depth of underwater receiver and the attenuation coefficient of water.

Fig. 3.3 shows the UAV energy consumption versus the depth of underwater receiver for the optimized LED transmit power obtained by Algorithm 1 in comparison with

Table 3.1: System parameters [41], [31]

Notation	Parameter	Value
$k\alpha$	Wave steepness	0.4
λ_w	Wavelength of water wave	1.3 m
$\|y_s\|$	Distance from transmitter to surface level	10 m
$\|y_g\|$	Distance from receiver to surface level	10 to 15 m
x_0	Underwater receiver localization accuracy	7 m
$P_{\max}$	Maximum LED transmit power	45.7 W
$P_{\min}$	Minimum LED transmit power	5.5 W
BER_{req}	Required bit error rate	1.5×10^{-3}
A	Receiving area of the underwater receiver	160 mm^2
k_w	Attenuation coefficient of water	0.25 to 0.45 m^{-1}
θ	LED angular beamwidth	45°
F_V	Field of view of the receiver	50 mrad
W	Downwelling irradiance	1440 W/m^2
R	Reflectance of downwelling irradiance	1.25%
L_f	Directional dependence of radiance	2.9
γ	Quantum efficiency of the detector	0.8
I_{DC}	Dark current of the photodiode	1.226×10^{-9} A
T_e	Equivalent temperature	290 K
F	Circuit noise figure	4
R_L	Load resistance	100 Ω
B	Bandwidth of the received light signal	50 kHz [24]
B_O	Optical filter bandwidth	50 nm
T_F	Optical filter transmissivity	55%
P_{UAV}	UAV propulsion power	178.4 W [78]
D	Data volume	8 Mbit
λ	Wavelength of light signal in water	349nm [77]
T_b	Bit interval	2×10^{-5}s

Table 3.2: Transmit power and power conversion efficiency [77]

Transmit power P_{TX} (W) for ten LZ4-00B215 LEDs	5.6	14.9	26	30	42.7	45.7
Power conversion efficiency η_p	0.46	0.37	0.32	0.28	0.23	0.22

three benchmarks: LED transmitting at the maximum power, LED transmitting at the minimum power, and LED transmitting at a random power level uniformly distributed in the range of $[P_{\min}, P_{\max}]$. We can see that the UAV energy consumption with the optimal transmit power obtained by Algorithm 1 is significantly lower than the UAV energy consumption achieved by the three benchmarks at all the considered underwater receiver depths. For the underwater receiver depth of 10 meters, transmitting at the optimized power can save up to 47% of UAV energy consumption as compared with transmitting at the maximum power. The UAV energy consumption under the minimum transmit power or the uniformly distributed transmit power dramatically grows as the depth of the underwater receiver increases because the required transmission time increases significantly. This is demonstrated in Fig. 3.4, which plots the required transmission time versus the depth of underwater receiver for the optimized transmit power and the three benchmarks. From Fig. 3.4 we can see that transmitting at the optimized power requires only slightly longer transmission time than transmitting at the maximum power, thus resulting in close-to-minimum propulsion energy consumption of the UAV, while significantly reducing the transmission energy consumption as compared with transmitting at the maximum power.

For analysis purposes, Fig. 3.5 shows the energy consumption of UAV and the required transmission time versus the LED transmit power for four different depths of the underwater receiver. We can see that for all the considered depths of underwater receiver, the UAV energy consumption first decreases and then slowly increases with the LED transmit power after reaching a minimum value, while the required transmission time rapidly decreases with the LED transmit power until reaching a minimum value. This can be explained as follows. When the LED transmit power is low, it requires a long time to transmit the given volume of data and the UAV energy consumption is dominated by propulsion energy consumption; when the LED transmit power in-

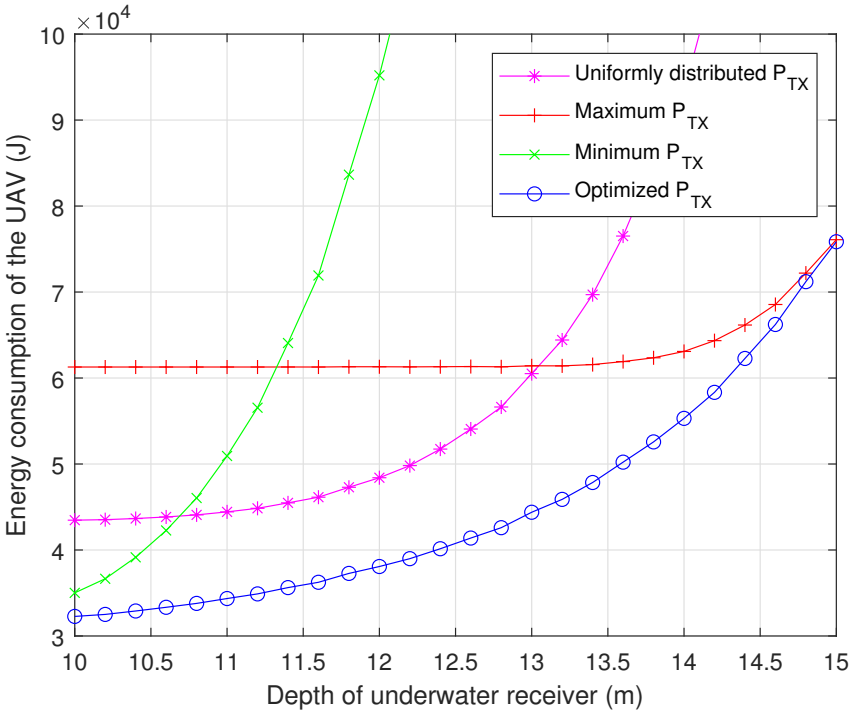

Figure 3.3: The energy consumption of the UAV versus the depth of underwater receiver.

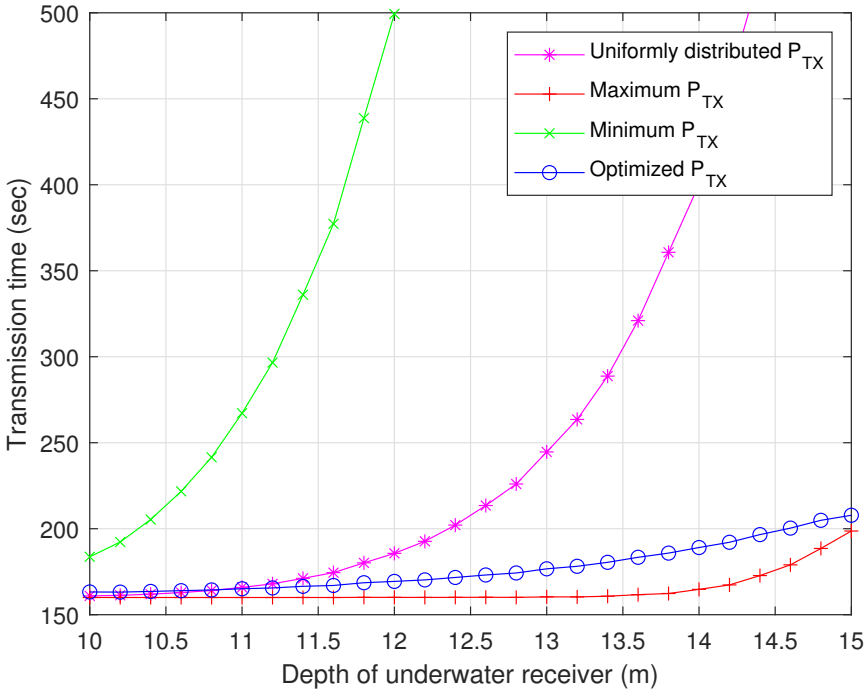

Figure 3.4: The required transmission time versus the depth of underwater receiver.

creases, the required transmission time decreases and so does the UAV propulsion energy consumption; however, the transmission time stops decreasing when the LED transmit power goes beyond a certain value because the transmission rate is limited by the OOK-NRZ channel capacity, and any further increase of the LED transmit power will lead to a higher transmission energy consumption of the UAV. It is interesting to note that for each considered depth of underwater receiver, the LED transmit power that minimizes the UAV energy consumption is lower than that minimizes the transmission time. This indicates that the minimum UAV energy consumption is achieved at the cost of the transmission time being slightly longer than the minimum possible value. The optimal LED transmit power that minimizes the UAV energy consumption increases with the depth of underwater receiver.

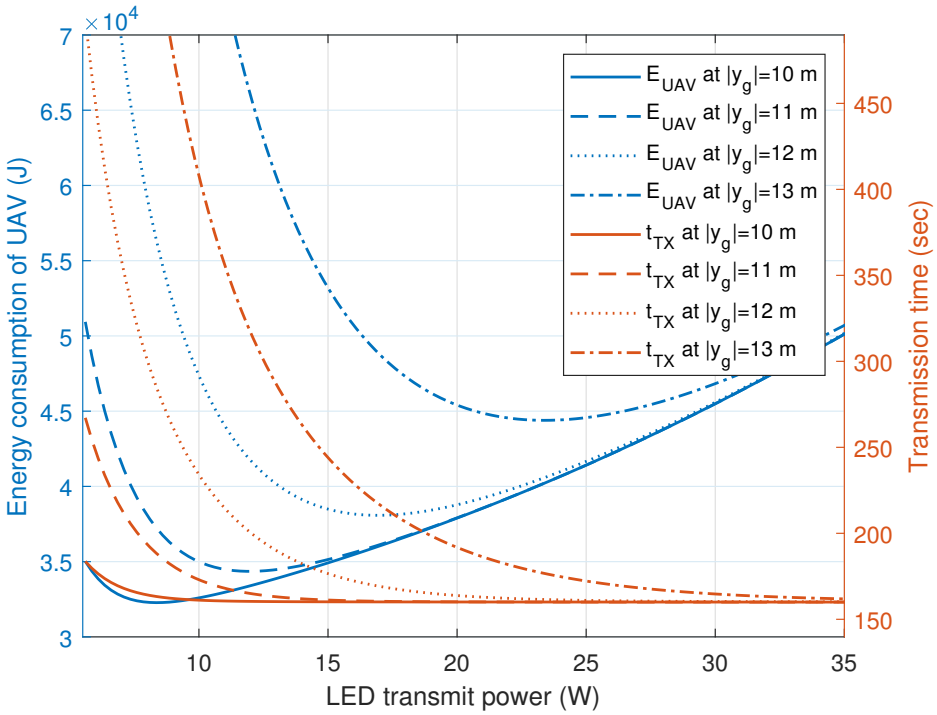

Figure 3.5: Energy consumption of UAV and transmission time versus the LED transmit power for different depths of underwater receiver.

3.6 Summary

In this chapter, an air-to-water visible light communication system is proposed, which includes a mathematical model of the water surface, light propagation path and various underwater noise terms. Based on the model, a SQP-based algorithm is devised to minimize the UAV energy consumption for transmitting a certain volume of data to an underwater receiver by optimizing the LED transmit power while ensuring the received SNR is above a threshold. The UAV energy consumption consists of the energy used for both the LED transmission and the UAV propulsion when hovering above the water. The simulation results show that the optimized LED transmit power and the energy consumption of the UAV both increase with the depth of the underwater receiver and the attenuation coefficient of water. For the underwater receiver depth of 10 meters, the LED transmit power optimized by the proposed algorithm can reduce the total energy consumption of the UAV by up to 47% as compared to that of LED transmitting at the maximum power.

Chapter 4

Energy Consumption Minimization of Water-to-air VLC

4.1 Overview

In this chapter, an water-to-air VLC system where an UAV carrying a photodiode receiver hovers above the water and receives VLC signals from an underwater LED transmitter is considered. In this system, a shallow water wave is considered, where the wavelength of the water surface wave is larger than the water depth.

4.2 Water-to-Air VLC System Model

4.2.1 Water Surface Model

The cross section of an water-to-air communication environment at a given time instant is plotted in the (x, y) plane in Fig. 4.1. According to Boussinesq equations and KdV [22] equation, the water surface elevation can be expressed as follows:

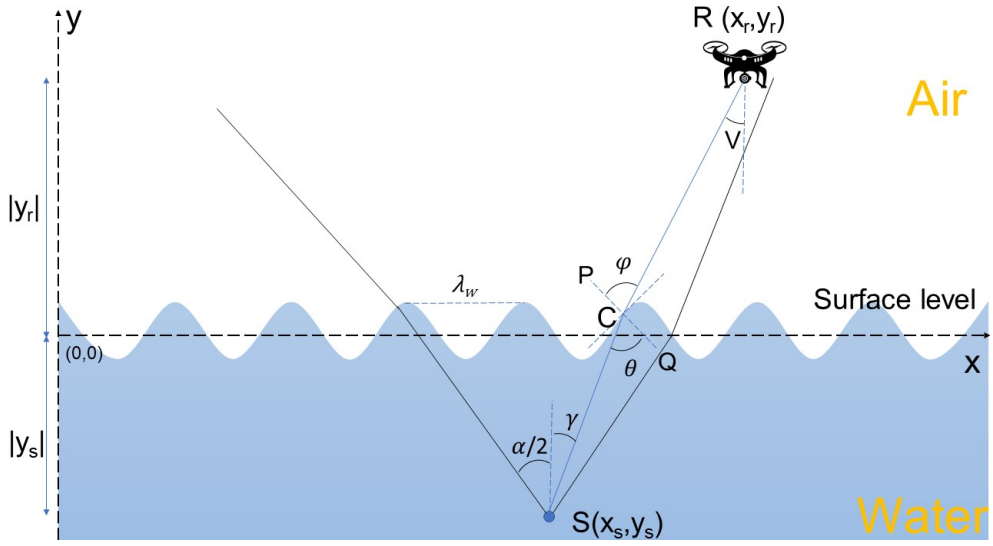

Figure 4.1: A cross section of the water-air interface.

$$f(x,t) = f_A + HJ^2\left(\frac{x - c_w t}{f_B}|m\right), \tag{4.1}$$

$$f_A = \frac{H}{m}\left[1 - m - \frac{E(m)}{K(m)}\right], \tag{4.1a}$$

$$f_B = \frac{\lambda_w}{2K(m)} = h\sqrt{\frac{4mh}{3H}}, \tag{4.1b}$$

$$c_w = \sqrt{gh}\left\{1 + \frac{H}{mh}\left[1 - \frac{m}{2} - \frac{3E(m)}{2K(m)}\right]\right\}, \tag{4.1c}$$

where x is the horizontal coordinate of a point on the water surface, t is time, H is wave height, J is the Jacobi DN elliptic function, c_w is phase speed of water wave, $m \in (0,1)$ is the square of elliptic modulus, $E(m)$ is the complete elliptic integral of the second kind, $K(m)$ is the complete elliptic integral of the first kind, λ_w is the wavelength of water wave, h is water depth and g is the gravitational acceleration.

$f(x,t)$ is periodic with respect to time t and its period T_w is given by [22]

$$T_w = \frac{\lambda_w}{c_w}. \tag{4.2}$$

4.2.2 Light Propagation Path

For analytical tractability, it is assumed that the underwater LED transmitter points upward vertically and the receiver at the UAV points downward vertically. Denote the positions of the underwater LED transmitter and the receiver at the UAV by S and R, respectively, then the coordinates of S and R in the (x,y) plane are (x_s,y_s) and (x_r,y_r), respectively. The UAV knows the default position of the underwater LED transmitter at (x_r,y_s) and hovers straight above it, but the underwater receiver may be drifted away from its default position by the water current. It is assumed that the underwater receiver is kept within a radius of x_0 from its default position at the water depth $|y_s|$ by a mooring cable [70].

The incident point of the light propagation path on the water surface is denoted by C with coordinates (x_c,y_c). According to Snell's law [49], the relationship between the incident angle θ and the refraction angle φ is given by:

$$n_w \sin(\theta) = n_a \sin(\varphi), \tag{4.3}$$

where n_w and n_a are the refractive index of water and air, respectively. The angles θ and φ can be calculated by utilizing the slopes of lines $\overline{\mathrm{SC}}$ and $\overline{\mathrm{CR}}$ and the normal line at the incident point C, similarly as (3.4)–(3.6), as follows:

$$\theta(t,\delta,x_s) = \tan^{-1}\left|\frac{[y_s - f(x_c,t)]\frac{\partial f(x_c,t)}{\partial x_c} + (x_s - x_c)}{(x_s - x_c)\frac{\partial f(x_c,t)}{\partial x_c} - y_s + f(x_c,t)}\right|, \tag{4.4}$$

$$\varphi(t,\delta,x_s) = \tan^{-1}\left|\frac{[y_r - f(x_c,t)]\frac{\partial f(x_c,t)}{\partial x_c} + (x_r - x_c)}{(x_r - x_c)\frac{\partial f(x_c,t)}{\partial x_c} - y_r + f(x_c,t)\Big)}\right|. \tag{4.5}$$

Substituting (4.4) and (4.5) into (4.3), (4.3) can be solved for x_c and then $y_c = f(x_c,t)$ can be obtained based on (4.1). When there are several solutions of x_c from solving (4.3), the proper solution is selected by checking whether or not the resulting slopes of lines $\overline{\mathrm{SC}}$ and $\overline{\mathrm{CR}}$ and the normal line at the incident point C are reasonable for light refraction. Substituting the proper x_c into (4.4) and (4.5), φ and θ can be obtained.

Let D_{SC} and D_{CR} denote the transmission distances underwater and above the water, respectively. They can be calculated by

$$D_{\mathrm{SC}}(t,\delta,x_s) = \sqrt{(x_c(t,\delta,x_s) - x_s)^2 + (y_c(t,\delta,x_s) - y_s)^2}, \tag{4.6}$$

$$D_{\mathrm{CR}}(t,\delta,x_s) = \sqrt{(x_c(t,\delta,x_s) - x_r)^2 + (y_c(t,\delta,x_s) - y_r)^2}. \tag{4.7}$$

The angle γ between the optical axis of the LED transmitter and $\overline{\mathrm{SC}}$, and the angle V between the optical axis of the receiver and $\overline{\mathrm{CR}}$, can be calculated by

$$\gamma(t,\delta,x_s) = \tan^{-1}\left|\frac{x_c(t,\delta,x_s) - x_s}{y_c(t,\delta,x_s) - y_s}\right|, \tag{4.8}$$

$$V(t,\delta,x_s) = \tan^{-1}\left|\frac{x_c(t,\delta,x_s) - x_r}{y_c(t,\delta,x_s) - y_r}\right|. \tag{4.9}$$

Other cross sections of the water-to-air communication environment can be obtained by rotating the cross section in Fig. 4.1 horizontally for an angle in the range from 0

to 180 degrees [41]. The water surface elevation function in the cross section that is rotated around the line of $x = x_s$ from the cross section containing $f(x,t)$ by an angle of δ is given by:

$$f(x',t) = f[x\cos(\delta), t], \tag{4.10}$$

where $x' = x\cos(\delta)$. The light propagation path in each new cross section can be obtained in a way similar to the above.

Let α denote the LED beam angle. For the worst case that $x_s = x_r - x_m$ or $x_s = x_r + x_m$, if $\gamma(t, \delta, x_r - x_m) \leq \frac{\alpha}{2}, \forall t, \delta$, then the receiver location $R(x_r, y_r)$ is in the light coverage at all times for all cross sections. Otherwise, in some cross sections, the light propagation path is not inside the LED beam and the receiver location may be outside the light coverage.

4.2.3 Received Light Power

Without loss of generality, it is assumed that the LED transmitter adopts the OOK-NRZ modulation, where the presence of a carrier (i.e., a constant positive light intensity) during a whole bit period represents a logic one and the absence of the carrier (i.e., zero light intensity) in a bit period represents a logic zero [53].

The transmitted information bits are recovered by the receiver using a matched filter for direct-detection [47]. The resulting electrical signal sampled at the output of the matched filter can be expressed as [48]:

$$Y_i = \eta I X_i + n_i, \tag{4.11}$$

where η is the optical-to-electrical conversion coefficient, I is the light intensity of the received signal, $X_i \in \{0, 1\}$ is the ith information bit, and n_i is the AWGN in the ith bit period. The AWGN has a zero mean and variance σ_n^2. According to [48], η is given

by:

$$\eta = \frac{pT_b q\lambda}{hc}, \tag{4.12}$$

where p is the quantum efficiency of the photodetector at the receiver, T_b is the bit interval, $q = 1.6 \times 10^{-19} coulombs$ is the elementary charge, $h = 6.6261 \times 10^{-34} J$ is Plank's constant, $c = 2.997 \times 10^8 m/s$ is the speed of light in the air, and λ is the wavelength of the light signal in the air.

In addition to refraction, the water surface also affects the transmittance due to reflection depending on the incident angle. Letting τ denote the transmittance, it is calculated according to Fresnel's equation [49] by:

$$\begin{aligned}\tau(t,\delta,x_s) = 1 &- \frac{\left|\frac{n_w cos[\theta(t,\delta,x_s)] - n_a cos[\varphi(t,\delta,x_s)]}{n_w cos[\theta(t,\delta,x_s)] + n_a cos[\varphi(t,\delta,x_s)]}\right|^2}{2} \\ &- \frac{\left|\frac{n_w cos[\varphi(t,\delta,x_s)] - n_a cos[\theta(t,\delta,x_s)]}{n_w cos[\varphi(t,\delta,x_s)] + n_a cos[\theta(t,\delta,x_s)]}\right|^2}{2}.\end{aligned} \tag{4.13}$$

Given the transmission distances underwater D_{SC} and in the air D_{CR}, as well as the transmittance τ, similarly as (3.17), the light intensity I at the receiver can be obtained according to Beer's law [49]:

$$I(t,\delta,x_s) = \frac{P_{\mathrm{TX}}\tau(t,\delta,x_s)e^{-k_w D_{\mathrm{SC}}(t,\delta,x_s)}}{2\theta D^2_{\mathrm{CR}}(t,\delta,x_s)}, \tag{4.14}$$

where P_{TX} is the LED transmit power and k_w is the attenuation coefficient of water that depends on the biological factors of water as well as the light wavelength. In a given underwater environment, k_w may vary with the depth of the observation point underwater. However, according to the measurement results in [74], the change of k_w

is negligible when it is measured at depths in the range from 10 to 30 meters (i.e., the euphotic zone of the ocean), which is the range of depths at which the target underwater LED transmitter is deployed, hence k_w is considered as a constant for simplicity.

The received power P_{RX} at the receiver carried by the UAV is then given by:

$$P_{\mathrm{RX}}(t, \delta, x_s) = I(t, \delta, x_s) A cos[V(t, \delta, x_s)], \tag{4.15}$$

where A is the receiving area of the receiver.

4.2.4 Received SNR

The receiver at the UAV is affected by the dark current noise, thermal noise, and shot noise [31] [24], which are assumed to follow independent zero-mean Gaussian distributions with variance of σ^2_{SS}, σ^2_{DC} and σ^2_{TH}, respectively. Hence, the variance σ^2_n of the noise term n_i is given by:

$$\sigma^2_n = \sigma^2_{\mathrm{SS}} + \sigma^2_{\mathrm{DC}} + \sigma^2_{\mathrm{TH}}. \tag{4.16}$$

Shot noise, also known as quantum noise, arises from the nature of photodetection and its variance is given by [31]:

$$\sigma^2_{\mathrm{SS}} = 2q\Re P_{\mathrm{RX}} B + 2qI_b B, \tag{4.17}$$

where the I_b is the background noise current.

Dark current noise is caused by the constant current that exists when no light is incident on the photodiode and its variance is given by [31]:

$$\sigma^2_{\mathrm{DC}} = 2qI_{\mathrm{DC}} B, \tag{4.18}$$

where I_{DC} is the dark current of the photodiode and its value depends on the structure of the p-n junction, the doping levels of the material, and the temperature of the photodiode.

Thermal noise is generated by the load resistor and its variance is given by [31]:

$$\sigma_{\mathrm{TH}}^2 = \frac{4k_B T_e F B}{R_L}, \tag{4.19}$$

where $k_B = 1.381 \times 10^{-23} J/K$ is the Boltzmann's constant, T_e is the equivalent temperature in K, F is the circuit noise figure and R_L is the load resistance.

The average SNR at the receiver carried by the UAV is expressed as [76]:

$$\begin{aligned} \rho &= \frac{\Re^2 P_{\mathrm{RX}}^2}{\sigma_n^2} \\ &= \frac{\Re^2 I^2 A^2 cos^2(V)}{\sigma_{\mathrm{SS}}^2 + \sigma_{\mathrm{DC}}^2 + \sigma_{\mathrm{TH}}^2}. \end{aligned} \tag{4.20}$$

4.2.5 Channel Capacity

For OOK-NRZ with direct detection at the receiver, the channel capacity in bit/pulse is given by [48]

$$\begin{aligned} C'_{\mathrm{OOK}}(t,\delta,x_s) = & \frac{\rho(t,\delta,x_s)}{2}\log_2(e) \\ & - \frac{e^{\frac{-\rho(t,\delta,x_s)}{4}}}{\sqrt{2\pi}} \int e^{\frac{-z^2}{2}} \cosh\left(z\sqrt{\frac{\rho(t,\delta,x_s)}{2}}\right) \\ & \times \log_2\left[\cosh\left(z\sqrt{\frac{\rho(t,\delta,x_s)}{2}}\right)\right] dz. \end{aligned} \tag{4.21}$$

Let T_b denote the bit interval. For time t, cross section with rotating angle δ and underwater LED transmitter position x_s, since the OOK-NRZ pulse rate is $1/T_b$

pulse/s, the channel capacity in bit/s is given by

$$C_{\mathrm{OOK}}(t,\delta,x_s)=\frac{1}{T_b}C'_{\mathrm{OOK}}(t,\delta,x_s). \tag{4.22}$$

We consider that forward error correction (FEC) with Bose–Chaudhuri–Hocquenghem (BCH) code is employed in the system with a code rate of 0.83 [79], the maximum possible net data rate is given by

$$R(t,\delta,x_s)=0.83\times C_{\mathrm{OOK}}(t,\delta,x_s). \tag{4.23}$$

For the considered FEC BCH scheme, the BER without FEC of 2×10^{-2} can be corrected to better than 1×10^{-12} [79]. Therefore, we consider the required BER for our system is $BER_{\mathrm{req}}=2\times10^{-2}$. For OOK-NRZ, the relationship between the BER and the received SNR is given by [76]

$$BER=\frac{1}{2}\operatorname{erfc}\left(\frac{1}{2\sqrt{2}}\sqrt{\rho}\right), \tag{4.24}$$

where erfc(.) is the complementary error function. Therefore, for the required BER, the required SNR is given by

$$\rho_{\mathrm{req}}=8\left[\operatorname{erfc}^{-1}\left(2BER_{\mathrm{req}}\right)\right]^2, \tag{4.25}$$

where $\operatorname{erfc}^{-1}(.)$ is the inverse complementary error function.

4.3 Problem Formulation

From (4.1), (4.4), (4.5), (4.6), (4.7), (4.9), (4.13)–(4.15), (4.20)–(4.23), we note that the water surface elevation function $f(x,t)$ is periodically varying with t and its has a

time period of T_w, which results periodic variations of transmission distances D_{SC} and D_{CR}, the transmittance τ, the light intensity I, the received power P_{RX}, the SNR at the receiver ρ, OOK-NRZ channel capacity C_{OOK}, and net data rate R with the same time period of T_w. From (4.4), (4.5), (4.6), (4.7), (4.9), (4.13)–(4.15), (4.20)–(4.23), D_{SC}, D_{CR} and V are functions of δ and x_s, which results τ, I, P_{RX}, ρ, C_{OOK} and R functions of δ and x_s. Therefore, for R, we have:

$$R(t, \delta, x_s) = R(t + T_w, \delta, x_s). \tag{4.26}$$

Let t_{TX} represent the time required to transmit M bits of data from an underwater LED transmitter to the UAV, which is defined as

$$M = \int_0^{t_{\mathrm{TX}}} R(t, \delta, x_s) dt. \tag{4.27}$$

Typically, t_{TX} is much larger than T_w, and it can be expressed as $t_{\mathrm{TX}} = NT_w + \varepsilon$, where N is an integer and $\varepsilon \in [0, T_w)$. We assume that the underwater LED transmitter needs to transmit a sufficiently large data volume and thus $t_{\mathrm{TX}} \gg T_w$, i.e., $\varepsilon \ll NT_w$. We can neglect ε and t_{TX} is given by

$$t_{\mathrm{TX}} \approx NT_w. \tag{4.28}$$

From (4.26), it holds that

$$\int_0^{T_w} R(t, \delta, x_s) dt = \int_{(n-1)T_w}^{nT_w} R(t, \delta, x_s) dt, \forall n \in \mathcal{Z}. \tag{4.29}$$

Substituting (4.28) and (4.29) into (4.27), M is rewritten as

$$M = N \int_0^{T_w} R(t, \delta, x_s) dt. \tag{4.30}$$

For the ease of exposition, we discretize T_w into L equal time slots each of Δt, i.e., $T_w = L\Delta t$, and let l denote the l^{th} time slot, $l \in U = \{1, \cdots, L\}$ for $t \in [0, T_w]$. We assume that Δt is appropriately chosen so that the capacity can be assumed to be approximately constant within each slot. From (4.30) and $T_w = L\Delta t$, M is reduced to

$$M = N \sum_{l=1}^{L} R(l\Delta t, \delta, x_s)\Delta t. \tag{4.31}$$

Then we have

$$N = \frac{M}{\sum_{l=1}^{L} R(l\Delta t, \delta, x_s)\Delta t}. \tag{4.32}$$

and

$$\begin{aligned} t_{\mathrm{TX}} &\approx NT_w \\ &= \frac{ML}{\sum_{l=1}^{L} R(l\Delta t, \delta, x_s)} \end{aligned} \tag{4.33}$$

Let η_p denote the LED's transmission power conversion efficiency, which may change with the transmit power of the LED and is usually given in the LED product specification. The power dissipation of the LED for data transmission is then P_{TX}/η_p. For any given rotating angle δ of the cross section and underwater LED transmitter position x_s, the energy consumption of the VLC system during the data transmission time, which consists of the power used for VLC by the underwater LED transmitter and the

propulsion power of the UAV when hovering above the water, is given by

$$E_{\text{sys}}(\delta, x_s) = \left(P_{\text{UAV}} + \frac{P_{\text{TX}}}{\eta_p}\right) t_{\text{TX}}, \\ \approx \frac{ML\left(P_{\text{UAV}} + \frac{P_{\text{TX}}}{\eta_p}\right)}{\sum_{l=1}^{L} R(l\Delta t, \delta, x_s)}, \tag{4.34}$$

where P_{UAV} denotes the constant propulsion power of the UAV for hovering at a fixed location.

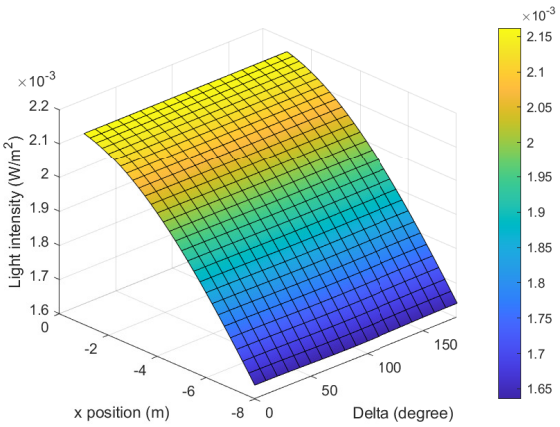

Figure 4.2: Light intensity versus the rotating angle and underwater LED transmitter position at $t = 0$.

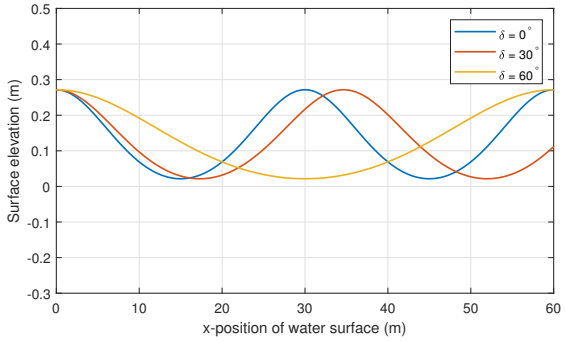

Figure 4.3: Surface elevation versus the x-position of water suface.

To minimize the energy consumption, we consider the worst case scenario among

all possible underwater LED transmitter positions $x_s \in [x_r - x_m, x_r + x_m]$ with waviest water surface elevation among all cross sections with rotating angle $\delta \in [0, \pi]$. From (4.6), (4.7), (4.13), a longer distance between the underwater LED transmitter position and its default position results in a larger transmission distance D_{SC} and D_{CR}, and from (4.14)–(4.23), (4.34), this will result in a smaller light intensity and channel capacity, thus lead to a higher energy consumption. This can be seem from Fig. 4.2, which present the light intensity versus the rotating angle and underwater LED transmitter position at $t = 0$, where the light intensity reach the minimum value at $x_s = x_r - x_m$ at any given δ, and the results are similar for any other given t. From Fig. 4.3, we can see that the worst water surface condition lays in $\delta = 0$, where the water wave is the heaviest. Therefore, the considered worst case energy consumption E'_{sys} is given by

$$E'_{\mathrm{sys}} = E_{\mathrm{sys}}(0, x_r - x_m). \tag{4.35}$$

Let $\gamma'(l)$ denote the angle between the optical axis of the LED transmitter and the light propagation direction underwater in time slot l for the considered worst case scenario, from (4.8), it is given by

$$\gamma'(l) = \gamma(l\Delta t, 0, x_r - x_m). \tag{4.36}$$

Let $\rho'(l)$ denote the OOK-NRZ channel capacity in time slot l for the considered worst case scenario, from (4.20), it is given by

$$\rho'(l) = \rho(l\Delta t, 0, x_r - x_m). \tag{4.37}$$

Our objective is to minimize the worst case energy consumption of the water-to-air VLC system by jointly optimizing the transmit power of the LED and the height of

the UAV, which is formulated as follows:

$$\text{(P0)}: \min_{P_{\text{TX}}, y_r} E'_{\text{sys}}, \tag{4.38}$$

$$\text{s.t. } \gamma'(l) \leq \frac{\alpha}{2}, \forall l, \tag{4.38a}$$

$$\rho'(l) \geq \rho_{\text{req}}, \forall l, \tag{4.38b}$$

$$P_{\min} \leq P_{\text{TX}} \leq P_{\max}, \tag{4.38c}$$

$$y_{r\_\min} \leq y_r \leq y_{r\_\max}, \tag{4.38d}$$

where $P_{\min}$ and $P_{\max}$ denote the minimum and maximum transmit power of the LED, respectively. Their values can be obtained from the LED product specification, e.g., [77]. $y_{r\_\min}$ and $y_{r\_\max}$ denote the minimum and maximum considered height of UAV. Constraint (4.38a) ensures that the receiver at the UAV is in the LED's light coverage at all times. Constraint (4.38b) ensures that the average SNR at the receiver at the UAV is above the required SNR ρ_{req} for a given BER.

4.4 Proposed Solution

In this section, we propose an alternating optimization algorithm for (P0) based on the block coordinate descent method and SQP algorithm. We choose the SQP algorithm because it is of a lower complexity than a metaheuristic algorithm for solving our minimization problem. It can be utilized through MATLAB minimization function 'fmincon'. Other iterative algorithms, such as active-set algorithm, are also appropriate for solving this minimization problem. Specifically, the proposed algorithm first optimizes the UAV height for given LED transmit power, and then optimizes the LED transmit power for given UAV height. This process is repeated alternately until convergence is reached.

Algorithm 2 The alternating optimization algorithm for (P0)

Input: $y_{r\_\min}, y_{r\_\max}, P_{\min}, P_{\max}, BER_{\text{req}}, \alpha, T_w, x_m$.
Set iteration index $i = 1$.
Initialize the LED transmit power P_{TX}^1.
Define the non-linear constraint function $\text{nonlcon}\left(y_r\right)$ and $\text{nonlcon}\left(P_{\text{TX}}\right)$ by using (4.38a), (4.38b), (4.38c) and (4.38d).
Solve (P1) for given P_{TX}^1 via the fmincon solver $\text{fmincon}\left[E'_{\text{sys}}\left(y_r\right), y_{r\_\min}, y_{r\_\max}, \text{nonlcon}\left(y_r\right), \text{SQP}\right]$, denote its solution as y_{r}^1, and calculate $E_{\text{sys}}^{\prime(1)}$ using (4.35).
repeat
  Update $i = i + 1$.
  Solve (P2) for given y_{r}^{i-1} via the fmincon solver $\text{fmincon}\left[E'_{\text{sys}}\left(P_{\text{TX}}\right), P_{\min}, P_{\max}, \text{nonlcon}\left(P_{\text{TX}}\right), \text{SQP}\right]$ and denote its solution as P_{TX}^i.
  Solve (P1) for given P_{TX}^i via the fmincon solver $\text{fmincon}\left[E'_{\text{sys}}\left(y_r\right), y_{r\_\min}, y_{r\_\max}, \text{nonlcon}\left(y_r\right), \text{SQP}\right]$ and denote its solution as y_{r}^i.
  Update $E_{\text{sys}}^{\prime(i)}$ based on y_{r}^i, P_{TX}^i using (4.35).
until $E_{\text{sys}}^{\prime(i-1)} - E_{\text{sys}}^{\prime(i)} \leq \epsilon$.
Output: The optimized UAV height $y_{\text{opt}} = y_{\text{r}}^i$ and the optimized LED transmit power $P_{\text{opt}} = P_{\text{TX}}^i$.

4.4.1 UAV Height Optimization

For a given underwater LED transmit power level, (P0) reduces to

$$\text{(P1)}: \min_{y_r} E'_{\text{sys}}, \tag{4.39}$$

$$\text{s.t. } (4.38\text{a}), (4.38\text{b}), (4.38\text{d}). \tag{4.40}$$

Since the objective and constraint functions are both continuous and have continuous first derivatives, (P1) is solved by standard optimization solvers that SQP algorithm (such as fmincon in MATLAB).

4.4.2 LED Transmit Power Optimization

For a given UAV height, (P0) reduces to

$$\text{(P2)}: \min_{P_{\text{TX}}} E'_{\text{sys}}, \tag{4.41}$$

$$\text{s.t. } (4.38a), (4.38b), (4.38c). \tag{4.42}$$

Since the objective and constraint functions are both continuous and have continuous first derivatives, (P2) is solved by standard optimization solvers that use SQP algorithm (such as fmincon in MATLAB).

4.4.3 Overall Algorithm Design

Based on the results presented in the previous two subsections, we propose an alternating optimization algorithm for (P0) by applying the block coordinate descent method. Specifically, (P0) are solved by alternately solving subproblems (P1) and (P2) until the changes in the system energy consumption between successive iterations are less than a threshold. The details of this algorithm are summarized in Algorithm 2. For the SQP algorithm, we recommend setting the initial point of the UAV height to $y_{r\_\min}$ for the SQP algorithm solving (P1) to help Algorithm 2 to converge to a optimized UAV height. The initial point of the LED transmit power for the SQP algorithm solving (P2) as well as for iteration 1 in Algorithm 2 can be set to any value in its feasible range.

Algorithm 2 is executed offline prior to the UAV deployment. After Algorithm 2 is done, the UAV is sent to hover at the optimized UAV height above the underwater transmitter. The value of optimized transmit power is informed by the UAV to the

underwater transmitter by air-to-water VLC link [80]. Finally, the underwater transmit start to transmit at the optimized transmit power to the UAV-carried receiver for the water-to-air VLC.

4.5 Results and Discussion

In this section, the simulation results are presented to evaluate the performance of the proposed Algorithm 2. In this simulation, the UAV DJI Phantom 4 RTK is chosen, which has a take-off weight of 1391g, battery capacity of 89.2 Wh and propulsion power of 178.4 W according to its specification [78]. Because blue-green light attenuates the least while propagating underwater, blue-green light LED LedEngin's LZ4-00B215 which has a dominant wavelength of 465nm in the air [77] and a wavelength of $\frac{n_a}{n_w} \times$ 465nm = 349nm in water [49] is considered in the simulation, and ten LZ4-00B215 LEDs in an array are arranged as the transmitter. It is assumed that the power consumption of carrying the receiver has been included in P_{UAV}.

The values of system parameters used in the simulation are listed in Table 4.1, where most of the parameter values are set following [41], [31]. For instance, the depth of underwater transmitter is considered to be in the range from 10 to 15 meters, and the UAV height is considered to be from 2 m to 20 m.

Fig. 4.4 shows the total energy consumption of the system versus the iteration number of Algorithm 2 at different depth of underwater LED transmitter and the attenuation coefficient of water. From the simulation results, Algorithm 2 converges by the second iteration for all the considered values of $|y_s|$ and k_w.

Fig. 4.5 shows the optimized total energy consumption of the system obtained by Algorithm 2 versus the depth of underwater LED transmitter as well as the attenuation coefficient of water. From Fig. 3.2, we can see that the optimized total energy con-

Table 4.1: System parameters [41], [31]

Notation	Parameter	Value
H	Wave height	0.5 m
h	Wave depth	15 m
m	The square of elliptic modulus	0.5
λ_w	Wavelength of water wave	30 m
$\|y_s\|$	Distance from transmitter to surface level	10 m to 15 m
y_{r_max}	Maximum UAV height	20 m
y_{r_min}	Minimum UAV height	2 m
x_0	Underwater transmitter localization accuracy	10 m
$P_{\max}$	Maximum LED transmit power	45.7 W
$P_{\min}$	Minimum LED transmit power	5.6 W
BER_{req}	Required bit error rate	2×10^{-2}
A	Receiving area of the receiver at the UAV	160 mm^2
k_w	Attenuation coefficient of water	0.2 to 0.45 m^{-1}
θ	LED angular beamwidth	45°
γ	Quantum efficiency of the detector	0.8
I_{DC}	Dark current of the photodiode	1.226×10^{-9} A
T_e	Equivalent temperature	290 K
F	Circuit noise figure	4
R_L	Load resistance	100 Ω
B	Bandwidth of the received light signal	50 kHz [24]
P_{UAV}	UAV propulsion power	178.4 W [78]
D	Data volume	8 Mb
λ	Wavelength of light signal in water	349nm [77]
T_b	Bit interval	2×10^{-5}s

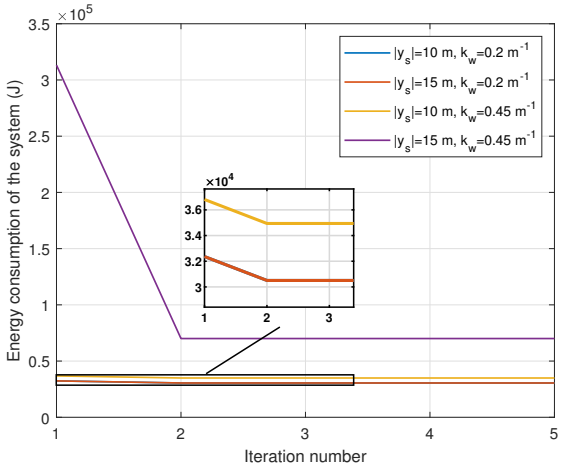

Figure 4.4: The total energy consumption of the system versus the iteration number at different depth of underwater LED transmitter and the attenuation coefficient of water

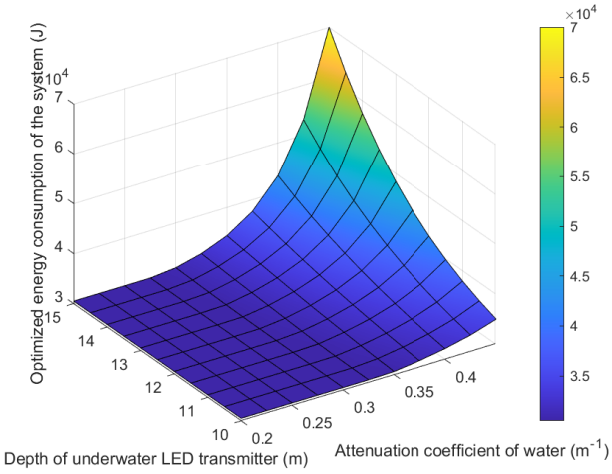

Figure 4.5: Optimized total energy consumption of the system versus the depth of underwater LED transmitter and the attenuation coefficient of water.

sumption of the system increases with the attenuation coefficient of water for a given depth of underwater LED transmitter. For a given attenuation coefficient of water, as the depth of underwater LED transmitter increases, even though the optimal UAV height is reduced to compensate the increase of total transmission distance, the proportion of transmission distance underwater is increased so that a larger LED transmit power is required, resulting an increased total energy consumption of the system.

For performance comparison, we consider four benchmarks: LED transmitting at the maximum power while the UAV height is optimized, LED transmitting at a random power level uniformly distributed in the range of $[P_{\min}, P_{\max}]$ while the UAV height is optimized, LED transmitting at the optimized power while the UAV height is uniformly distributed in the range of $[y_{r\_\min}, y_{r\_\max}]$, and LED transmitting at a random power level uniformly distributed in the range of $[P_{\min}, P_{\max}]$ while the UAV height is uniformly distributed in the range of $[y_{r\_\min}, y_{r\_\max}]$.

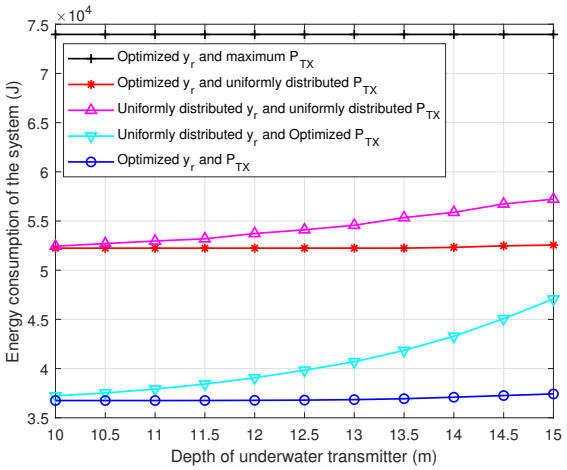

Figure 4.6: The total energy consumption of the system versus the depth of underwater LED transmitter for $k_w = 0.3\text{m}^{-1}$.

Fig. 4.6 shows the total energy consumption of the system versus the depth of underwater LED transmitter for the optimized UAV height and LED transmit power obtained by Algorithm 2 in comparison with the benchmarks. We can see that for all

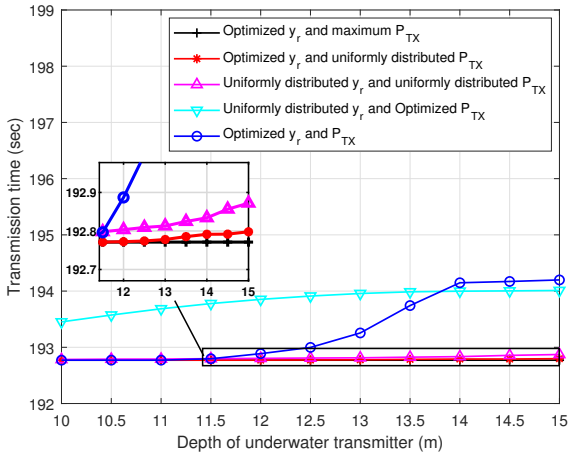

Figure 4.7: The required transmission time versus the depth of underwater LED transmitter for $k_w = 0.3\text{m}^{-1}$.

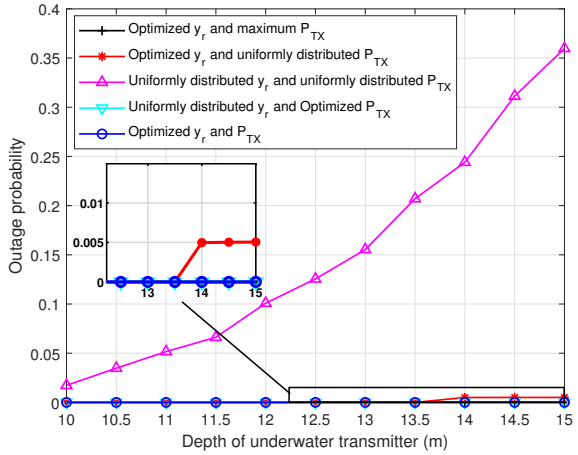

Figure 4.8: The outage probability versus the depth of underwater LED transmitter for $k_w = 0.3\text{m}^{-1}$.

the considered schemes, the total energy consumption of the system increases with the depth of the underwater LED transmitter because the underwater transmission distance becomes larger. The total energy consumption of the system with the optimized UAV height and LED transmit power is always lower than all the benchmarks for all the considered depth of underwater transmitter. The total energy consumption for transmitting at the maximum power level and the optimized UAV height remains constant for all the considered depths of the underwater transmitter. This is because the transmission rate reaches the OOK-NRZ channel capacity and the transmission time reaches its minimum. The reasons are the same for LED transmitting at uniformly distributted power level and optimized UAV height as well as the optimized UAV height and LED transmit power at shallow depths of underwater transmitter. For depths of underwater transmitter larger than 13.5 m, the total energy consumption of the system for the former two strategies start to increase because the transmission rate decreases with the large depth of the underwater transmitter even for the maximum LED transmit power and the required transmission time increases. This is also reflected in Fig. 4.7, which shows the required transmission time versus the depth of underwater LED transmitter for the optimized UAV height and LED transmit power obtained by Algorithm 2 in comparison with the benchmarks. From Fig. 4.7, transmitting at the maximum power level and optimized UAV height always achieve the minimum transmission time for all the considered depths of underwater transmitter. Transmitting at the optimized UAV height and LED transmit power requires slightly longer transmission time than transmitting at the maximum power and optimized UAV height, since it found the optimum in the trade-off between saving the transmission time to reduce the propulsion energy consumption of the UAV and saving the VLC transmission energy consumption, thus resulting in a significant lower of total energy consumption of the system with minor sacrificing of transmission time especially for shallow depths of

underwater transmitter.

Fig. 4.8 shows the outage probability versus the depth of underwater LED transmitter for different benchmarks. The outage is defined as the either constraint (3.32a) or (3.32b) is not met. We can see that the outage probabilities for optimized UAV height and LED transmit power, optimized UAV height and LED transmitting at the maximum power level, and uniformly distributed UAV height and optimized LED transmit power are all zero. The outage probability for uniformly distributed UAV height and uniformly distributed LED transmit power is relatively high and increases with the depth of underwater transmitter. It rises to around 36% at underwater transmitter depth of 15m.

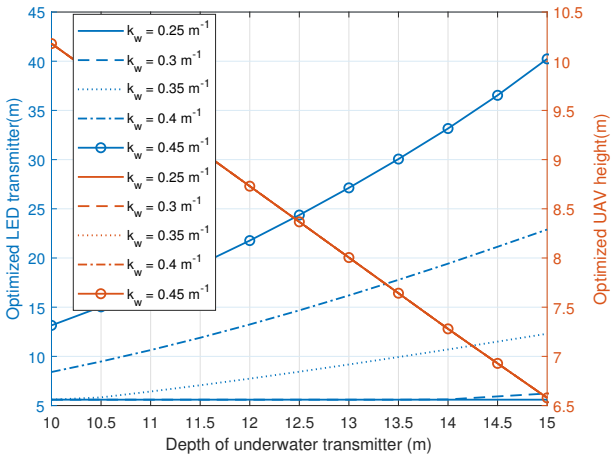

Figure 4.9: Optimized LED transmit power and UAV height versus the depth of underwater LED transmitter.

Fig. 4.9 shows the optimized LED transmit power and the optimized UAV height obtained by Algorithm 2 versus the depth of underwater LED transmitter for different attenuation coefficient of water. We can see that the optimized UAV height decreases with the depth of underwater LED transmitter, but does not vary with the attenuation coefficient of water. This is because by applying Algorithm 2, the UAV height is always optimized to as low as possible while still in light coverage to reach maximum

transmission rate. The optimized LED transmit power increases with the the depth of underwater LED transmitter and the attenuation coefficient of water. For a larger attenuation coefficient of water, the optimized LED transmit power increases faster with the depth of the underwater transmitter.

4.6 Summary

In this chapter, an water-to-air VLC system is proposed, which includes a mathematical model of the water surface, light propagation path and various underwater noise terms. The energy consumption formula is derived by solving the transmission time for the LED transmitter to transmit a certain amount of data to the receiver. The energy consumption minimization problem is formulated in the worst-case scenario and jointly optimizes the LED transmit power and the UAV height. The proposed algorithm outperforms four other benchmarks in saving the total energy consumption of the system. It saves the total energy consumption of the system by around 32% compared to transmitting at a random power level and UAV hovering at a random height.

Chapter 5

Conclusions and Future Work

5.1 Conclusions

In this thesis, the air-water DLOS VLC systems are analysed, where the energy consumption problems are mainly focused. Specifically, the work that have been done is concluded as follows.

In Chapter 3, an low-power air-to-water DLOS VLC system is studied, where an LED transmitter carried by an UAV hovering above the water needs to transmit a certain volume of data to an underwater receiver in a deep water scenario. The deep water air-water interface is mathematically modelled by Stokes's third-order theory and the light incident point on the water surface is analytically derived for a given UAV position and all possible positions of the underwater receiver that fall inside the light coverage. After analysing the underwater noise at the receiver and deriving the SNR at the receiver and channel capacity, the formulated energy consumption minimization problem is solved by the proposed SQP-based algorithm by by optimizing the LED transmit power.

In Chapter 4, the low power water-to-air DLOS VLC system, where an underwater

LED transmitter sends optical signal to a receiver carried by the UAV above the water in a shallow water scenario. The shallow water air-water interface is mathematically modelled by using Boussinesq equations and KdV [22] equation. To extend the work of air-to-water VLC system in chapter 3, the UAV height is further considered as the optimizing parameter since it is a controllable parameter when deploying the UAV. For the formulated energy consumption minimization problem of the system that including the UAV propulsion power and the energy consumption by VLC link, the LED transmit power and the UAV height are jointly optimized by the proposed algorithm.

For both work in air-water VLC, the propose algorithm outperforms the other benchmark strategies of choosing the LED transmit power or the UAV height in minimizing the energy consumption while keeping the transmission time at the same level. Specifically, in the air-to-water VLC system, for the underwater receiver depth of 10 meters, the optimized LED transmit power can reduce the total energy consumption of the UAV by up to 47% as compared to that of LED transmitting at the maximum power, and in the water-to-air VLC system, for the underwater transmitter depth of 10 meters, the optimal values of the LED transmit power and the UAV height can save around 32% of the total energy consumption of the system as compared with transmitting at a random power level and placing the UAV at a random height.

5.2 Future Work

This thesis could be extended in various directions. Some of the potential future topics based on this thesis are summarized in the following.

5.2.1 Two-Way Air-Water VLC

Two-way air-water VLC system model could be extended from this thesis, where one or multiple UAVs and AUVs carrying VLC transceivers communication with each other across the air-water interface. This is enabled by that the light can transmit directly between the air and the water without much variations.

In the two-way air-water VLC link, the transceiver includes a LED or a laser as the transmitter and an APD as the receiver. Alignment issue for a two-way air-water VLC link will be more challenging, especially for laser-based transmitter, than an one-way VLC link, since both of the transceivers at the UAV and the AUV need to be in the light coverage area of each other.

Many recent works have modelled and experimental studied the two-way air-water VLC systems [37,55,63,65]. Nevertheless, the mathematical water surface model is usually neglected and the energy-related problem are not considered. Therefore, extending the works in Chapters 3 and 4 to two-way air-water VLC link would be an interesting topic for future research. After mathematically modelling the air-water surface, the light coverage areas for both the UAVs and the AUVs can be analysed. To minimise the energy consumption of a two-way air-water VLC system, the propulsion power of the UAVs and the AUVs need to be considered as well as the energy consumption by the VLC link.

5.2.2 Beam Tracking

Beam tracking is studied in recent works for the air-water VLC system [34] and the vehicular VLC system [81]. In such VLC links that the transmission nodes is mobility, beam tracking helps the transmitter(or the receiver) to locate the receiver(or the transmitter) and achieve a better alignment especially for the laser-based VLC and the

VLC using a LED with narrow beam. By using beam tracking, the UAV continuously emits brief but high-energy pulses to locate and monitor the AUV by measuring the reflections of these pulses. Subsequently, a gimbal tracker mounted on the UAV sweeps across the AUV's surface to locate its optical lens and align the laser link.

Therefore, applying beam tracking to extend the work in this thesis enables the real time position adjustment of the UAV. Compared with applying the algorithm offline before dispatching the UAV, using tracking procedure in real time to locate the underwater node which may be drift away from its default position can reduce the transmission distance while ensuring it in the light coverage area, and finally results in a lower energy consumption of the VLC system.

5.2.3 Air-Water VLC Under Strong Turbulence

For the works in Chapter 3 and 4, a weak turbulence scenario is considered where the impact of the turbulence can be neglectable. To extend the works to the scenario that the turbulence is significant strong, the effect of turbulence needs to be considered. There are many works study the turbulence in the water [27–29, 50–52]. However, the current models are not mature and mostly based on laboratory experiments. Finding and applying a mathematically turbulence model to this thesis can be more realistic and accurate in understanding the underwater path loss and therefore minimizing the energy consumption of the system especially for a significant turbulence water scenario.

References

[1] F. S. Alqurashi, A. Trichili, N. Saeed, B. S. Ooi, and M.-S. Alouini, "Maritime communications: A survey on enabling technologies, opportunities, and challenges," *IEEE Internet of Things Journal*, vol. 10, no. 4, pp. 3525–3547, 2023.

[2] H. Luo, X. Xie, G. Han, R. Ruby, F. Hong, and Y. Liang, "Multimodal acoustic-rf adaptive routing protocols for underwater wireless sensor networks," *IEEE Access*, vol. 7, pp. 134 954–134 967, 2019.

[3] H. Lei, Y. Zhang, K.-H. Park, I. S. Ansari, G. Pan, and M.-S. Alouini, "Performance analysis of dual-hop rf-uwoc systems," *IEEE Photonics Journal*, vol. 12, no. 2, pp. 1–15, 2020.

[4] A. Samir, M. Elsayed, A. A. A. El-Banna, I. Shafique Ansari, K. Rabie, and B. M. ElHalawany, "Performance analysis of dual-hop hybrid rf-uowc noma systems," *Sensors*, vol. 22, no. 12, 2022.

[5] D. Pompili and I. F. Akyildiz, "Overview of networking protocols for underwater wireless communications," *IEEE Communications Magazine*, vol. 47, no. 1, pp. 97–102, 2009.

[6] B. Xu, L. Qiu, and J. Yang, "Analysis of time delay and error compensation for multi-auvs cooperative navigation approach," *Control and Decision*, vol. 30, no. 1, pp. 9–16, 2015.

[7] E. Moorits and A. Usk, "Buoy collision detection," in *Proceedings ELMAR-2012*, 2012, pp. 109–112.

[8] M. S. Islam, M. Younis, and A. Ahmed, "Communication through air water interface using multiple light sources," in *2018 IEEE International Conference on Communications (ICC)*, 2018, pp. 1–6.

[9] B. Chai, X. Zhang, and J. Wang, "A test of magnetic induction communication from air to sea," in *2018 OCEANS - MTS/IEEE Kobe Techno-Oceans (OTO)*, 2018, pp. 1–4.

[10] Z. Tian, X. Zhang, and H. Wei, "A test of cross-border magnetic induction communication from water to air," in *2020 IEEE International Conference on Signal Processing, Communications and Computing (ICSPCC)*, 2020, pp. 1–4.

[11] M. C. Watson, J.-F. Bousquet, and A. Forget, "Evaluating the feasibility of magnetic induction to cross the air-water boundary," in *2021 Fifth Underwater Communications and Networking Conference (UComms)*, 2021, pp. 1–4.

[12] M. Muzzammil, N. Ahmed, G. Qiao, I. Ullah, and L. Wan, "Fundamentals and advancements of magnetic-field communication for underwater wireless sensor networks," *IEEE Transactions on Antennas and Propagation*, vol. 68, no. 11, pp. 7555–7570, 2020.

[13] H. Wang and Y. Ren, "Em wave propagation through the seawater-air interface in dynamic marine environment," in *Global Oceans 2020: Singapore – U.S. Gulf Coast*, 2020, pp. 1–4.

[14] S. Yang, J. Geng, H. Zhou, K. Wang, X. Zhao, J. Lu, R. Zhao, X. Tang, Y. Zhang, D. Su, A. Zhang, H. Li, and R. Jin, "Long-range em communication underwater with ultracompact elf magneto-mechanical antenna," *IEEE Transactions on Antennas and Propagation*, vol. 71, no. 3, pp. 2082–2097, 2023.

[15] F. Tonolini and F. Adib, "Networking across boundaries: Enabling wireless communication through the water-air interface," in *Proceedings of the 2018 Conference of the ACM Special Interest Group on Data Communication*. New York, NY, USA: Association for Computing Machinery, 2018, p. 117–131.

[16] Y. Zhao, P. Li, P. Zhang, Z. Zhou, and J. Li, "Application of laser-induced acoustic method on air-underwater communication," in *2021 International Conference on Space-Air-Ground Computing (SAGC)*, 2021, pp. 77–82.

[17] J. Luo, X. Pan, and L. Cheng, "Characterizing laser-induced acoustic signals based on thermal expansion mechanism: Simulation studies and experiment verifications," in *2021 6th International Conference on Communication, Image and Signal Processing (CCISP)*, 2021, pp. 295–302.

[18] P. Nabavi, A. F. M. S. Haq, and M. Yuksel, "Empirical modeling and analysis of water-to-air optical wireless communication channels," in *2019 IEEE International Conference on Communications Workshops (ICC Workshops)*, 2019, pp. 1–6.

[19] H. Luo, J. Wang, F. Bu, R. Ruby, K. Wu, and Z. Guo, "Recent progress of air/water cross-boundary communications for underwater sensor networks: A review," *IEEE Sensors Journal*, vol. 22, no. 9, pp. 8360–8382, 2022.

[20] L. E. M. Matheus, A. B. Vieira, L. F. M. Vieira, M. A. M. Vieira, and O. Gnawali, "Visible light communication: Concepts, applications and challenges," *IEEE Communications Surveys & Tutorials*, vol. 21, no. 4, pp. 3204–3237, 2019.

[21] M. Davies and A. K. Chattopadhyay, "Stokes waves revisited: Exact solutions in the asymptotic limit," *The European Physical Journal Plus*, vol. 131, 2016.

[22] A. K. Piotr Rozmej and E. Infeld, "Superposition solutions to the extended kdv equation for water surface waves," *Nonlinear Dynamics*, vol. 91, pp. 1085–1093, 2018.

[23] C. Yang and F. Yang, "Communication interruption analysis for air-water wireless optical communication," in *International Wireless Communications and Mobile Computing (IWCMC)*, 2023, pp. 1022–1027.

[24] J. Giles and I. Bankman, "Underwater optical communications systems. part 2: basic design considerations," in *IEEE Military Communications Conference(MILCOM)*, vol. 3, 2005, pp. 1700–1705.

[25] H. Kaushal and G. Kaddoum, "Underwater optical wireless communication," *IEEE Access*, vol. 4, pp. 1518–1547, 2016.

[26] D. J. Bogucki, J. A. Domaradzki, D. Stramski, and J. R. Zaneveld, "Comparison of near-forward light scattering on oceanic turbulence and particles," *Appl. Opt.*, vol. 37, no. 21, pp. 4669–4677, Jul 1998.

[27] X. Sun, C. H. Kang, M. Kong, O. Alkhazragi, Y. Guo, M. Ouhssain, Y. Weng, B. H. Jones, T. K. Ng, and B. S. Ooi, "A review on practical considerations and solutions in underwater wireless optical communication," *J. Lightwave Technol.*, vol. 38, no. 2, pp. 421–431, Jan 2020.

[28] W. Liu, Z. Xu, and L. Yang, "Simo detection schemes for underwater optical wireless communication under turbulence," *Photon. Res.*, vol. 3, no. 3, pp. 48–53, Jun 2015.

[29] M. Sharifzadeh and M. Ahmadirad, "Performance analysis of underwater wireless optical communication systems over a wide range of optical turbulence," *Optics Communications*, vol. 427, pp. 609–616, 2018.

[30] Y. Zhao, A. Wang, L. Zhu, W. Lv, J. Xu, S. Li, and J. Wang, "Performance evaluation of underwater optical communications using spatial modes subjected to bubbles and obstructions," *Opt. Lett.*, vol. 42, no. 22, pp. 4699–4702, Nov 2017.

[31] S. Jaruwatanadilok, "Underwater wireless optical communication channel modeling and performance evaluation using vector radiative transfer theory," *IEEE Journal on Selected Areas in Communications*, vol. 26, no. 9, pp. 1620–1627, 2008.

[32] X. Sun, M. Kong, C. Shen, C. H. Kang, T. K. Ng, and B. S. Ooi, "On the realization of across wavy water-air-interface diffuse-line-of-sight communication based on an ultraviolet emitter," *Opt. Express*, vol. 27, no. 14, pp. 19 635–19 649, Jul 2019.

[33] C. Fu, C. Gong, N. Huang, J. Luo, and Z. Xu, "Concatenated rs-ldpc coding for water-to-air visible light communication through wavy water surface," in *2021 13th International Conference on Wireless Communications and Signal Processing (WCSP)*, 2021, pp. 1–5.

[34] Y. Di, Y. Shao, and L.-K. Chen, "Real-time wave mitigation for water-air owc systems via beam tracking," *IEEE Photonics Technology Letters*, vol. 34, no. 1, pp. 47–50, 2022.

[35] M. Li, P. Ling, S. Wen, X. Chen, and F. Wen, "Bubble-wave-mitigation algorithm and transformer-based neural network demodulator for water-air optical camera communications," *IEEE Photonics Journal*, vol. 15, no. 5, pp. 1–10, 2023.

[36] Q. Hu, C. Gong, T. Lin, J. Luo, and Z. Xu, "Secrecy performance analysis for water-to-air visible light communication," *Journal of Lightwave Technology*, vol. 40, no. 14, pp. 4607–4620, 2022.

[37] Q. Hu, N. Huang, and C. Gong, "Superposition modulation for physical layer security in water-to-air visible light communication systems," *Journal of Lightwave Technology*, vol. 41, no. 10, pp. 2976–2990, 2023.

[38] S. Guan, J. Wang, C. Jiang, R. Duan, Y. Ren, and T. Q. S. Quek, "Magicnet: The maritime giant cellular network," *IEEE Communications Magazine*, vol. 59, no. 3, pp. 117–123, 2021.

[39] A. M. Khasawneh, O. Kaiwartya, A. Khalifeh, L. M. Abualigah, and J. Lloret, "Green computing in underwater wireless sensor networks pressure centric energy modeling," *IEEE Systems Journal*, vol. 14, no. 4, pp. 4735–4745, 2020.

[40] A. Dallolio, B. Agdal, A. Zolich, J. A. Alfredsen, and T. A. Johansen, "Long-endurance green energy autonomous surface vehicle control architecture," in *OCEANS 2019 MTS/IEEE SEATTLE*, 2019, pp. 1–10.

[41] M. S. Islam and M. F. Younis, "Analyzing visible light communication through air–water interface," *IEEE Access*, vol. 7, pp. 123 830–123 845, 2019.

[42] J. D. Fenton, "A fifth-order stokes theory for steady waves," *Journal of Waterway, Port, Coastal, and Ocean Engineering*, vol. 111, no. 2, pp. 216–234, 1985.

[43] L.-K. Chen, Y. Shao, and Y. Di, "Underwater and water-air optical wireless communication," *Journal of Lightwave Technology*, vol. 40, no. 5, pp. 1440–1452, 2022.

[44] J. Tessendorf *et al.*, "Simulating ocean water," *Simulating nature: realistic and interactive techniques. SIGGRAPH*, vol. 1, no. 2, p. 5, 2001.

[45] A. A. Abrashkin, Pelinovsky, and E. Naumovich, "Gerstner waves and their generalizations in hydrodynamics and geophysics," *Physics Uspekhi*, vol. 65, pp. 453–467, 2022.

[46] J. Kahn and J. Barry, "Wireless infrared communications," *Proceedings of the IEEE*, vol. 85, no. 2, pp. 265–298, 1997.

[47] J. Dang, L. Wu, and Z. Zhang, "Ofdm systems for optical communication with intensity modulation and direct detection," *Optical fiber and wireless communications*, vol. 85, pp. 111–117, 2017.

[48] J. S. Everett *et al.*, "Forward-error correction coding for underwater free-space optical communication," Raleigh, North Carolina, 2009.

[49] M. Born and E. Wolf, *Principles of Optics*. Cambridge University Press, 1999.

[50] M. Elamassie and M. Uysal, "Performance characterization of vertical underwater vlc links in the presence of turbulence," in *2018 11th International Symposium on Communication Systems, Networks & Digital Signal Processing (CSNDSP)*, 2018, pp. 1–6.

[51] M. Wang, X. Yuan, O. AlHarbi, P. Deng, and T. Kane, "Propagation of laser beams through air-sea turbulence channels," in *Laser Communication and Propagation through the Atmosphere and Oceans VII*, J. P. Bos, A. M. J. van Eijk, and S. Hammel, Eds., vol. 10770, International Society for Optics and Photonics. SPIE, 2018, p. 1077003.

[52] J. Li, J. Luo, S. Li, and X. Yuan, "Centroid drift of laser beam propagation through a water surface with wave turbulence," *Appl. Opt.*, vol. 59, no. 20, pp. 6210–6217, Jul 2020.

[53] H. J. R. Dutton, "Optical communication systems," in *Understanding optical communications*. Prentice Hall PTR, 1998, pp. 297–350.

[54] C. J. Carver, Z. Tian, Q. Shao, H. Zhang, K. M. Odame, A. Q. Li, and X. Zhou, "Air-water communication and sensing with light," in *14th International Conference on Communication Systems & Networks (COMSNETS)*, 2022, pp. 371–374.

[55] J. P. Kachhadiya and A. Kashyap, "Air-water optical communication using an airborne radio controlled aircraft," in *2018 Second International Conference on Intelligent Computing and Control Systems (ICICCS)*, 2018, pp. 631–635.

[56] N. Huang, C. Gong, C. Fu, T. Wei, and Z. Xu, "Preliminary investigation of air-to-water visible light communication link under strong ambient light," in *2021 IEEE 94th Vehicular Technology Conference (VTC2021-Fall)*, 2021, pp. 1–5.

[57] F. Blackmon and L. Antonelli, "Experimental detection and reception performance for uplink underwater acoustic communication using a remote, in-air, acousto-optic sensor," *IEEE Journal of Oceanic Engineering*, vol. 31, no. 1, pp. 179–187, 2006.

[58] W. Wang, J. Long, L. Zheng, S. Qiao, J. Lu, and L. Huang, "Realization of two-way communication across the air-water interface by thermoacoustic effect," in *2022 IEEE MTT-S International Microwave Biomedical Conference (IMBioC)*, 2022, pp. 198–200.

[59] R. S. Sangeetha, R. L. Awasthi, and T. Santhanakrishnan, "Design and analysis of a laser communication link between an underwater body and an air platform," in *2016 International Conference on Next Generation Intelligent Systems (ICNGIS)*, 2016, pp. 1–5.

[60] X. Sun, M. Kong, O. A. Alkhazragi, K. Telegenov, M. Ouhssain, M. Sait, Y. Guo, B. H. Jones, J. S. Shamma, T. K. Ng, and B. S. Ooi, "Field demonstrations of wide-beam optical communications through water–air interface," *IEEE Access*, vol. 8, pp. 160 480–160 489, 2020.

[61] T. Lin, N. Huang, C. Gong, J. Luo, and Z. Xu, "Preliminary characterization of coverage for water-to-air visible light communication through wavy water surface," *IEEE Photonics Journal*, vol. 13, no. 1, pp. 1–13, 2021.

[62] T. Lin, C. Fu, T. Wei, N. Huang, X. Liu, L. Tang, L. Su, J. Luo, and C. Gong, "Waving effect characterization for water-to-air optical wireless communication," *Journal of Lightwave Technology*, vol. 41, no. 1, pp. 120–136, 2023.

[63] K. Enhos, E. Demirors, D. Unal, and T. Melodia, "Software-defined visible light networking for bi-directional wireless communication across the air-water interface," in *2021 18th Annual IEEE International Conference on Sensing, Communication, and Networking (SECON)*, 2021, pp. 1–9.

[64] A. Wang, L. Zhu, Y. Zhao, S. Li, W. Lv, J. Xu, and J. Wang, "Adaptive water-air-water data information transfer using orbital angular momentum," *Opt. Express*, vol. 26, no. 7, pp. 8669–8678, Apr 2018.

[65] P. Agheli, H. Beyranvand, and M. J. Emadi, "Uav-assisted underwater sensor networks using rf and optical wireless links," *Journal of Lightwave Technology*, vol. 39, no. 22, pp. 7070–7082, 2021.

[66] J. B. Saif, M. Younis, F.-S. Choa, and A. Ahmed, "Localization of autonomous underwater vehicles using airborne visible light communication links," in *32nd Wireless and Optical Communications Conference (WOCC)*, 2023, pp. 1–6.

[67] M. Kong, J. Lin, C. H. Kang, C. Shen, Y. Guo, X. Sun, M. Sait, Y. Weng, H. Zhang, T. K. Ng, and B. S. Ooi, "Toward self-powered and reliable visible light communication using amorphous silicon thin-film solar cells," *Opt. Express*, vol. 27, no. 24, pp. 34 542–34 551, Nov 2019.

[68] Z. Ji, Y. Fu, J. Li, Z. Zhao, and W. Mai, "Photoacoustic communication from the air to underwater based on low-cost passive relays," *IEEE Communications Magazine*, vol. 59, no. 1, pp. 140–143, 2021.

[69] R. M. Hagem, S. G. O'Keefe, T. Fickenscher, and D. V. Thiel, "Self contained adaptable optical wireless communications system for stroke rate during swimming," *IEEE Sensors Journal*, vol. 13, no. 8, pp. 3144–3151, 2013.

[70] S.-M. Yoon, C.-M. Lee, K. Kim, and S.-H. Byun, "Pitch and depth keeping of moored-type underwater acoustic array system," in *OCEANS 2019 MTS/IEEE SEATTLE*, 2019, pp. 1–4.

[71] W. Zhang, G. Han, X. Wang, M. Guizani, K. Fan, and L. Shu, "A node location algorithm based on node movement prediction in underwater acoustic sensor networks," *IEEE Transactions on Vehicular Technology*, vol. 69, no. 3, pp. 3166–3178, 2020.

[72] Y. Ata and Y. Baykal, "Scintillations of optical plane and spherical waves in underwater turbulence," *Journal of the Optical Society of America*, vol. 31, no. 7, pp. 1552–1556, Jul 2014.

[73] S. A. Thorpe, *The Turbulent Ocean*. Cambridge University Press, 2005.

[74] L. J. Johnson, R. J. Green, and M. S. Leeson, "Underwater optical wireless communications: depth dependent variations in attenuation," *Applied Optics*, vol. 52, no. 33, pp. 7867–7873, Nov 2013.

[75] G. J. Edelman, R. J. Hoveling, M. Roos, T. G. van Leeuwen, and M. C. Aalders, "Infrared imaging of the crime scene: Possibilities and pitfalls," *Journal of Forensic Sciences*, vol. 58, no. 5, pp. 1156–1162, 2013.

[76] A. M. Ibrahimy, B. I. Fadilah, and B. Pamukti, "Analysis of modulation performance of underwater visible light communication with variable wavelength," in *2020 3rd International Conference on Information and Communications Technology (ICOIACT)*, 2020, pp. 451–455.

[77] *High luminous efficacy blue power LedFlex™ emitter LZ4-00B215*, LedEngin, Inc., 2023, available at https://www.farnell.com/datasheets/87098.pdf.

[78] *Phantom 4 RTK Specs*, DJI., 2023, available at Available:https://www.dji.com/gr/phantom-4-rtk/info.

[79] T. Mizuochi, K. Kubo, H. Yoshida, H. Fujita, H. Tagami, M. Akita, and K. Motoshima, "Next generation fec for optical transmission systems," in *OFC 2003 Optical Fiber Communications Conference, 2003.*, vol. 2, 2003, pp. 527–528.

[80] W. Du, Y. Liu, N. Tang, and X. Chu, "Energy consumption minimization of air-to-water visible light communications," in *TechRxiv*, 2023.

[81] W. Jiang, X. Jin, Y. Zhang, M. Jin, C. Gong, and Z. Xu, "Trajectory prediction of target light source for dynamic visible light communication systems with a narrow field of view," in *2020 IEEE International Conference on Communications Workshops (ICC Workshops)*, 2020, pp. 1–6.